Annexin A2 depletion exacerbates the intracerebral microhemorrhage induced by acute rickettsia and Ebola virus infections

Zhengchen Su[1], Qing Chang[1], Aleksandra Drelich[1], Thomas Shelite[2], Barbara Judy[1], Yakun Liu[1], Jie Xiao[1], Changchen Zhou[1], Xi He[1], Tais Saito[1,5], Shaojun Tang[3], Lynn Soong[4,5], Maki Wakamiya[6], Xiang Fang[6], Alexander Bukreyev[1,4,5], Thomas Ksiazek[1,5], William K. Russell[7], Bin Gong[1,5,*]

1Department of Pathology, University of Texas Medical Branch, Galveston, Texas 77555, USA.

[2]Department of Internal Medicine, Infectious Diseases, University of Texas Medical Branch, Galveston, Texas 77555, USA.

[3]Department of Neuroscience and Cell Biology, University of Texas Medical Branch, Galveston, Texas 77555, USA.

[4]Department of Microbiology and Immunology, University of Texas Medical Branch, Galveston, Texas 77555, USA.

[5]Glveston National Laboratory, Galveston, Texas 77555, USA.

[6]Department of Neurology, University of Texas Medical Branch, Galveston, Texas 77555, USA.

[7]Department of Biochemistry and Molecular Biology, University of Texas Medical Branch, Galveston, Texas 77555, USA.

[*]Correspondence to: Bin Gong, MD, PhD, Tel. 409-772-2877; Fax. 409-266-6810; Email: bigong@utmb.edu.

Keywords: Annexin A2, intracerebral microhemorrhage, ZO-1, occludin, rickettsia, Ebola virus, proteomics.

Abstract

Intracerebral microhemorrhages (CMHs) are small foci of hemorrhages in the cerebrum. Acute infections induced by some intracellular pathogens, including rickettsia, can result in CMHs. Annexin a2 (ANXA2) has been documented to play a functional role during intracellular bacterial adhesion. Here we report that *ANXA2*-knockout (KO) mice are more susceptible to CMHs in response to rickettsia and Ebola virus infections, suggesting an essential role of ANXA2 in protecting vascular integrity during these intracellular pathogen infections. Proteomic analysis via mass spectrometry of whole brain lysates and brain-derived endosomes from *ANXA2*-KO and wild-type (WT) mice post-infection with *R. australis* revealed that a variety of significant proteins were differentially expressed, and the follow-up function enrichment analysis had identified

several relevant cell-cell junction functions. Immunohistology study confirmed that both infected WT and infected *ANXA2*-KO mice were subjected to adherens junctional protein (VE-cadherin) damages. However, key blood-brain barrier (BBB) components, tight junctional proteins ZO-1 and occludin, were disorganized in the brains from *R. australis*-infected *ANXA2*-KO mice, but not those of infected WT mice. Similar *ANXA2*-KO dependent CMHs and fragments of ZO-1 and occludin were also observed in Ebola virus-infected *ANXA2*-KO mice, but not found in infected WT mice. Overall, our study revealed a novel role of ANXA2 in the formation of CMHs during *R. australis* and Ebola virus infections; and the underlying mechanism is relevant to the role of ANXA2-regulated tight junctions and its role in stabilizing the BBB in these deadly infections.

Author Summary

Traditionally, spontaneous intracerebral microhemorrhages (CMHs) were defined as small foci of intracerebral hemorrhages. Such atraumatic CMHs are due to the rupture of a weak blood vessel wall. Infections complicating cerebrovascular accidents have been extensively investigated. However, the role of CMHs complicating infections, in particularly acute systemic infections, has been poorly explored. Population-based retrospective cohort studies suggest there are potentially more undiscovered cases of CMHs accompanying acute systemic infections. Given both the lack of an animal model and cellular/molecular pathophysiology of CMHs following acute systemic infections, there is an urgent need to increase our comprehensive understanding of acute infection-induced CMHs. Overall, our study revealed a novel role of annexin a2 (ANXA2) in the formation of CMHs during *R. australis* and Ebola virus infections; and the underlying mechanism is relevant to the role of ANXA2-regulated endothelial tight junctions and its role in stabilizing the blood-brain barrier in these deadly infections.

Introduction

Spontaneous intracerebral microhemorrhages (CMHs) are defined as small foci of hemorrhages in the cerebrum [1-3]. These atraumatic CMHs are due to the rupture of small arteries, arterioles, and/or capillaries[4]. CMHs have been a frequently recognized entity since the widespread application of magnetic resonance imaging[1, 5]. Recent investigations into CMHs have seen notable developments, and the increasing prevalence of CMHs is recognized as a significant problem [1, 2]. A population-based retrospective cohort study revealed that 18% of patients with central nervous system (CNS) infections developed CMHs within one year after the initial infection, 47 times greater than non-CNS infection controls[6]. Infections complicating

cerebrovascular accidents have been extensively investigated[7-26]. However, the role of CMHs complicating infections[27-30], in particular, acute infections, has been poorly explored[6, 31-33]. To the best of our knowledge, four clinic reports from different countries described a total of 11 cases of CMH after acute systemic infections in patients ranging in age from 9 to 71 years[34-37]. Nine cases in two reports correlated the CMHs with specific pathogen infections, spotted fever (SF) rickettsiosis or ehrlichiosis[37]. Taken together, this information suggests there are potentially more undiscovered cases of CMHs accompanying acute systemic infections.

CMH can be acutely caused by pathogen-associated inflammation (AICMHs)[32, 38]. One of the underlying pathology of AICMHs is the acute dysfunction of the blood-brain barrier (BBB)[39] which is the interface between circulating blood and the central nervous system (CNS) and is composed of brain microvascular endothelial cells (BMECs), pericytes, and astrocytes[40, 41]. BBB properties are primarily determined by junctional complexes between the BMECs, i.e. adherens junctions (AJs) and tight junctions (TJs)[42-44]. Several infectious agents, including rickettsia and Ebola virus, can directly or indirectly target brain endothelial barrier function. Rickettsioses represent devastating human infections[45]. These arthropod-borne diseases are caused by obligate intracellular bacteria of the genus *Rickettsia spp* (*R.*)[46-51]. Disseminated infection of vascular endothelial cell (EC) and endothelial barrier dysfunction are the central pathophysiologic features of human lethal spotted fever group rickettsiosis (SFGR) [45, 46, 52-55]. Ebola virus is associated with severe hemorrhagic diseases in humans. Similar to rickettsia, Ebola virus targets both the immune system[56-63] and ECs, causing severe vascular leakage syndrome[64-68], but the underlying mechanisms remain unclear. Two main mechanisms have been proposed: the virus infects macrophages and dendritic cells, which then release cytokines to activate ECs; and/or the virus directly infects and activates ECs[67, 69].

Annexin A2 (ANXA2) is a member of the large annexin family of Ca^{2+}-regulated and phospholipid-binding proteins, which associates with cell membrane dynamics, cell-cell interactions, and cell adhesion[70-76]. ANXA2 can be monomeric, found mainly in the cytosol, or forming heterotetramer complex with S100A10 [72, 77]. S100A10 is a unique member of S100 protein family that has been known to bind to ANXA2. The interaction between ANXA2 and S100A10 yields a heterotetramer complex ANXA2-S100A10, enabling ANXA2 to translocate across the EC membrane and perform a variety of functions, facilitating plasmin-based fibrinolytic activities on vascular luminal surfaces[71, 72, 78]. Recently, we identified host ANXA2 as a novel

receptor for SFGR and staphylococcus aureus adhesions to ECs[79]. However, there was no difference in rickettsial adhesion to or invasion into white blood cells between the wild-type (WT) and *ANXA2*-knockout (KO) mice.

Here we report an observation that focal CMH lesions exist in the cerebra of *R. australis* infected *AXNA2*-KO mice but not *R. australis* infected WT mice. We hypothesize cell-cell junction in the BBB is destabilized in *AXNA2*-KO mice rendering them susceptible to AICMH. In order to comprehensively investigate this possibility, we performed a proteomic analysis using the whole brain lysate and brain-derived isolated endosomes. We identified a variety of differentially expressed (DE) proteins that were relevant to vascular integrity. Functional group annotation and network analysis based on the identified DE proteins revealed a variety of protein functional group changes, such as cell-cell junction, stress fiber, MHC II protein complex binding, and stress response. These identified functional groups support that a structural impairment of the BBB might be involved. Consistently, immunofluorescence (IF) of brain tissue of *R. australis* infected mice revealed dramatic disruption and disorganization of TJ proteins ZO-1 and occludin in *ANXA2*-KO mice, but not WT mice. Interestingly, *ANXA2*-KO mice challenged by Ebola virus also exhibited CMHs and aberrant TJs whereas WT mice showed no signs of bleeding into CNS, indicating this pathology is not specific to rickettsia infection. Collectively, these data suggest that ANXA2 is required for the integrity of TJs in response to acute rickettsia and Ebola infections.

Results

1. Absence of ANXA2 is associated with the incidence of CMH in *R. australis* infection.

To investigate the potential role of *ANXA2*-KO on survival of the mice in response to the *R. australis* infection, WT (n=14) and *ANXA2*-KO (n=15) mice were inoculated with an ordinary lethal dose of *R. australis* (2×10^6) via tail vein injection (i.v.) [79, 80] and observed up to 10 days post-infection (p.i.). Accumulative survival data were obtained from three independent experiments (**Supplemental Fig. 1A**) and subjected to Kaplan-Meier (K-M) analysis. We found no difference in survival between WT (21.43%) and *ANXA2*-KO (13.33%) groups. However, the gross pathology of the brain surface (**Supplemental Fig. 1B**) observed apparent different color cerebral areas between infected WT mice and infected *ANXA2*-KO. To examine underlying associated pathology(s), brain tissue sections were subjected to histological examination with hematoxylin and eosin (H&E) staining (**Fig. 1**), which revealed striking focal CMHs, in the cerebra of all lethally infected *ANXA2*-KO mice (**Fig. 1G-L**), but not in the two survival infected *ANXA2*-

KO mice. Conversely, such CMHs were absent from both lethal and survival WT infected mice (**Fig. 1 D-F**).

2. Inactivation of ANXA2 does not affect the proliferation of *R. australis* and serum levels of IFNγ and TNFα in mice.

For time-dependent pathological studies, mice were inoculated with an ordinary lethal dose of *R. australis* (2 x 10^6). At 5 days p.i. (5 mice per group), both *ANXA2*-KO and WT mice were euthanized as designed. H&E examination revealed extensive focal hemorrhagic lesions, at levels of arteriole, capillary, and venule, in the cerebra of all infected *ANXA2*-KO mice on day 5 p.i., but not WT mice (**Fig. 2A-D**).

To examine whether ANXA2 plays a role in serum levels of IFNγ and TNFα during the lethal dose of *R. australis* infection, serum from mice at day 2, 4, or 5 p.i. were collected and proceeded to analyze the concentration of IFNγ and TNFα. However, no difference was found comparing WT and *ANXA2*-KO mice (**Fig. 2E and F**). Furthermore, on day 5 post-infection, the real-time qPCR analysis revealed no difference in bacterial loads in brain between WT (n=4) and *AXNA2*-KO mice (n=4) (**Fig. 2G**). Immunofluorescent staining (IF) of rickettsia in the liver, brain and lung did not show any difference between WT and *ANXA2*-KO mice on day 5 p.i. (**Fig. 3**). These data suggest *ANXA2* depletion does not affect the overall proliferation of *R. australis* in the mice.

3. Proteomic analysis.

In order to decipher the protein profile related to the CMHs observed in the *ANXA2*-KO mice post rickettsia infection, we performed a proteomic analysis of the whole brain protein lysate and isolated endosome. Isolated endosome protein pattern is important due to the involvement of ANXA2 in endocytosis and turnover of surface proteins and nucleotide[72].

3.1 *Whole-brain lysate*

Comparing the protein profiles of brain lysate from *ANXA2*-KO and WT mice challenged by *R.australis* infection on day 5 p.i., LC/MS analysis identified one hundred thirty DE, with 93 upregulated and 37 downregulated (*ANXA2*-KO versus WT). The top upregulated and downregulated proteins are listed in **Tables 1 & 2**. It is noteworthy that the hemoglobin level was higher (4-fold) in the infected *ANXA2*-KO mice, suggesting to be the cause of different gross pathology from the infected WT mice. Functional enrichment analysis and visualization (**Fig. 4 & 6**) revealed statistically significant functional groups that are potentially associated with CMH in *ANXA2*-KO mice. The noteworthy upregulated proteins that are associated with the cell junction

structure integrity include heat shock protein 90 α (HSP90α), heat shock protein 90 beta, enolase 1, clathrin (heavy polypeptide); important downregulated proteins include myosin (heavy polypeptide 10).

Table 1. Upregulated proteins and their KEGG pathway interpretation from whole-brain lysate. Fold change is calculated as (KO-WT)/WT.

Gene ID	Protein	Fold change	KEGG Pathway
AT2B1_MOUSE	ATPase, Ca++ transporting, plasma membrane 1(Atp2b1)	4.17	Calcium signaling pathway, cGMP-PKG signaling pathway, cAMP signaling pathway, Adrenergic signaling in cardiomyocytes, Salivary secretion, Pancreatic secretion,
Q3UHH0_MOUSE, AT2B2_MOUSE	ATPase, Ca++ transporting, plasma membrane 2(Atp2b2)	6.25	Calcium signaling pathway, cGMP-PKG signaling pathway, cAMP signaling pathway, Adrenergic signaling in cardiomyocytes, Salivary secretion, Pancreatic secretion,
VATA_MOUSE	ATPase, H+ transporting, lysosomal V1 subunit A(Atp6v1a)	4.36	Oxidative phosphorylation, Metabolic pathways, Phagosome, Synaptic vesicle cycle, Collecting duct acid secretion, Rheumatoid arthritis,
AP1B1_MOUSE	adaptor protein complex AP-1, beta 1 subunit(Ap1b1)	5.00	Lysosome,
CLH1_MOUSE	clathrin, heavy polypeptide (Hc)(Cltc)	5.83	Lysosome, Endocytosis, Synaptic vesicle cycle, Endocrine and other factor-regulated calcium reabsorption, Huntington's disease, Bacterial invasion of epithelial cells,
ENOA_MOUSE	enolase 1, alpha non-neuron(Eno1)	4.33	Glycolysis / Gluconeogenesis, Metabolic pathways, Biosynthesis of antibiotics, Carbon metabolism, Biosynthesis of amino acids, RNA degradation, HIF-1 signaling pathway,
HS90B_MOUSE	heat shock protein 90 alpha (cytosolic), class B member 1(Hsp90ab1)	4.10	Protein processing in endoplasmic reticulum, PI3K-Akt signaling pathway, Antigen processing and presentation, NOD-like receptor signaling pathway, Progesterone-mediated oocyte maturation, Estrogen signaling pathway, Pathways in cancer, Prostate cancer,

HS90A_MOUSE	heat shock protein 90, alpha (cytosolic), class A member 1(Hsp90aa1)	9.40	Protein processing in endoplasmic reticulum, PI3K-Akt signaling pathway, Antigen processing and presentation, NOD-like receptor signaling pathway, Progesterone-mediated oocyte maturation, Estrogen signaling pathway, Pathways in cancer, Prostate cancer,
A8DUK4_MOUSE	hemoglobin, beta adult s chain(Hbb-bs)	4.09	African trypanosomiasis, Malaria,
H2B1B_MOUSE	histone cluster 1, H2bb(Hist1h2bb)	4.67	Alcoholism, Viral carcinogenesis, Systemic lupus erythematosus,
H2B1K_MOUSE	histone cluster 1, H2bk(Hist1h2bk)	4.67	Alcoholism, Viral carcinogenesis, Systemic lupus erythematosus,
Q8CBB6_MOUSE	histone cluster 1, H2bq(Hist1h2bq)	4.67	Alcoholism, Viral carcinogenesis, Systemic lupus erythematosus,
MDHM_MOUSE	malate dehydrogenase 2, NAD (mitochondrial)(Mdh2)	11.75	Citrate cycle (TCA cycle), Cysteine and methionine metabolism, Pyruvate metabolism, Glyoxylate and dicarboxylate metabolism, Metabolic pathways, Biosynthesis of antibiotics, Carbon metabolism,
PFKAM_MOUSE	phosphofructokinase, muscle(Pfkm)	4.25	Glycolysis / Gluconeogenesis, Pentose phosphate pathway, Fructose and mannose metabolism, Galactose metabolism, Metabolic pathways, Biosynthesis of antibiotics,
KPYM_MOUSE	pyruvate kinase, muscle(Pkm)	8.83	Glycolysis / Gluconeogenesis, Purine metabolism, Pyruvate metabolism, Metabolic pathways, Biosynthesis of antibiotics, Carbon metabolism, Biosynthesis of amino acids,
SNP25_MOUSE	synaptosomal-associated protein 25(Snap25)	4.33	Synaptic vesicle cycle, Insulin secretion,
1433E_MOUSE	tyrosine 3-monooxygenase/tryptophan 5-monooxygenase activation protein, epsilon polypeptide(Ywhae)	4.17	Cell cycle, Oocyte meiosis, PI3K-Akt signaling pathway, Hippo signaling pathway, Neurotrophin signaling pathway, Viral carcinogenesis,

Table 2. Downregulated proteins and their KEGG pathway interpretation from whole-brain lysate. Fold change is calculated as (KO-WT)/WT.

Gene ID	Protein name	Fold change	Representative KEGG Pathway
A4GZ26_MOUSE, E9QAD8_MOUSE, D3Z5I6_MOUSE	IQ motif and Sec7 domain 2(Iqsec2)	-0.63	Endocytosis,
D3YZU5_MOUSE	SH3/ankyrin domain gene 1(Shank1)	-0.7	Glutamatergic synapse,

KCC2G_MOUSE	calcium/calmodulin-dependent protein kinase II gamma(Camk2g)	-0.63	ErbB signaling pathway, Calcium signaling pathway, cAMP signaling pathway, HIF-1 signaling pathway,
E9Q1T1_MOUSE, A0A0G2JGS4_MOUSE	calcium/calmodulin-dependent protein kinase II, delta(Camk2d)	-0.76	ErbB signaling pathway, Calcium signaling pathway, cAMP signaling pathway, HIF-1 signaling pathway,
MYH10_MOUSE, Q5SV64_MOUSE, Q3UH59_MOUSE	myosin, heavy polypeptide 10, non-muscle(Myh10)	-0.78	Tight junction,
PCLO_MOUSE	piccolo (presynaptic cytomatrix protein)(Pclo)	-0.76	Insulin secretion,

Functional enrichment analysis was performed based on Gene Ontology (GO) Term and Kyoto Encyclopedia of Genes and Genomes (KEGG) pathway. Noteworthy GO Term include *cell-cell adherens junction, stress fiber, actin cytoskeleton, MHC class II protein complex binding, vesicle-mediated transport, and extracellular vesicle.* In KEGG pathway, we identified a variety of signaling pathways, in which *PI3K-Akt signaling pathway, cAMP signaling pathway, and protein digestion and absorption pathway* may be relevant to the pathology of CMHs. The potential interacting network of DE proteins is shown in **Fig. 6**.

3.2 *Brain-derived isolated endosome*

The endosome is integral to the endocytosis pathway. Due to the nature of endosomes, the proteins enriched in the endosomes is either subjected to degradation or recycled back to the plasma membrane[81]. Increased accumulation of proteins in the endosomal compartment suggests increased protein turnover rate and degradation; whereas reduction of protein enrichment in the endosomes might result in protein accumulation in another compartment such as cytosol or plasma membrane[81].

ANXA2 is known to be associated with the endosomal membrane. Endocytosis of several targets depends on the presence of tyrosine phosphorylation of ANXA2[82-87]. The absence of ANXA2 may lead to a differential endosomal protein profile, which may shed light on the underlying mechanisms associated with the increased susceptibility of *ANXA2*-KO mice to CMH upon rickettsia infection.

Comparing the endosomes isolated from the mouse brains of WT mice and *ANXA2*-KO 5 days after rickettsial infection, we have identified 47 DE proteins, with 18 upregulated proteins, and 29 downregulated proteins in the infected *ANXA2*-KO mice. Noteworthy upregulated DE proteins

include talin1, alanyl-tRNA synthetase, glutathione peroxidase 1, and calcium/calmodulin-dependent protein kinase IV. Important downregulated proteins are cofilin 2, heat shock protein 8, HSP90α, thimet oligopeptidase and seryl-aminoacyl-tRNA synthetase. Top proteins are listed in **Table 3 & 4**. Functional enrichment analysis was performed based on these 47 DE proteins, generating a list of functional enriched clusters (**Fig. 5 & 7**). Noteworthy Go Term functional groups include cell-cell AJ, metalloproteinase, and MHC II protein complex binding. Significantly altered signaling pathways in KEGG are pyruvate metabolism, biosynthesis of antibiotics, metabolic pathways, caron metabolism, valine&leucine&isoleucine degradation, synthesis and degradation of ketone bodies.

Table 3. Upregulated proteins and their KEGG pathway interpretation from brain-derived endosomes. Fold change is calculated as (KO-WT)/WT.

ID	Gene Name	fold change	KEGG_PATHWAY
HMGCL_MOUSE	3-hydroxy-3-methylglutaryl-Coenzyme A lyase(Hmgcl)	2	Synthesis and degradation of ketone bodies, Valine, leucine and isoleucine degradation, Butanoate metabolism, Metabolic pathways, Peroxisome,
L1CAM_MOUSE	L1 cell adhesion molecule(L1cam)	2.5	Axon guidance, Cell adhesion molecules (CAMs),
SHLB2_MOUSE	SH3-domain GRB2-like endophilin B2(Sh3glb2)	2.33	Endocytosis,
AP2B1_MOUSE	adaptor-related protein complex 2, beta 1 subunit(Ap2b1)	3.5	Endocytosis, Synaptic vesicle cycle, Endocrine and other factor-regulated calcium reabsorption, Huntington's disease,
SYAC_MOUSE	alanyl-tRNA synthetase(Aars)	2.17	Aminoacyl-tRNA biosynthesis,
PYGB_MOUSE	brain glycogen phosphorylase(Pygb)	4.5	Starch and sucrose metabolism ,Metabolic pathways, Insulin signaling pathway, Glucagon signaling pathway,Insulin resistance,
KCC4_MOUSE	calcium/calmodulin-dependent protein kinase IV(Camk4)	2	Calcium signaling pathway, cAMP signaling pathway, Osteoclast differentiation, Long-term potentiation, Neurotrophin signaling pathway, Cholinergic synapse, Oxytocin signaling pathway, Aldosterone synthesis and secretion, Amphetamine addiction, Alcoholism,
GPX1_MOUSE	glutathione peroxidase 1(Gpx1)	3	Glutathione metabolism, Arachidonic acid metabolism,Thyroid hormone synthesis,
PGP_MOUSE	phosphoglycolate phosphatase(Pgp)	3	Glyoxylate and dicarboxylate metabolism, Metabolic pathways, Biosynthesis of antibiotics, Carbon metabolism,
TLN1_MOUSE	talin 1(Tln1)	3.33	Rap1 signaling pathway, Focal adhesion, Platelet activation, HTLV-I infection,

Table 4. Downregulated proteins and their KEGG pathway interpretation from brain-derived endosomes. Fold change is calculated as (KO-WT)/WT.

ID	Gene Name	Fold change	Representative KEGG_PATHWAY
CNDP2_MOUSE	CNDP dipeptidase 2 (metallopeptidase M20 family)(Cndp2)	-0.6	Arginine and proline metabolism, Histidine metabolism, beta-Alanine metabolism, Metabolic pathways,
UGPA_MOUSE	UDP-glucose pyrophosphorylase 2(Ugp2)	-0.75	Pentose and glucuronate interconversions, Galactose metabolism, Starch and sucrose metabolism, Amino sugar and nucleotide sugar metabolism, Metabolic pathways, Biosynthesis of antibiotics,
THIL_MOUSE	acetyl-Coenzyme A acetyltransferase 1(Acat1)	-0.67	Fatty acid degradation, Synthesis and degradation of ketone bodies, Valine, leucine and isoleucine degradation, Lysine degradation, Tryptophan metabolism, Pyruvate metabolism,
AL7A1_MOUSE	aldehyde dehydrogenase family 7, member A1(Aldh7a1)	-0.71	Glycolysis / Gluconeogenesis, Ascorbate and aldarate metabolism,Fatty acid degradation, Glycine, serine and threonine metabolism, Valine, leucine and isoleucine degradation, Lysine degradation,
BHMT1_MOUSE	betaine-homocysteine methyltransferase(Bhmt)	-0.67	Glycine, serine and threonine metabolism, Cysteine and methionine metabolism, Metabolic pathways,
COF2_MOUSE	cofilin 2, muscle(Cfl2)	-0.63	Axon guidance, Fc gamma R-mediated phagocytosis, Regulation of actin cytoskeleton,Pertussis,
LGUL_MOUSE	glyoxalase 1(Glo1)	-0.62	Pyruvate metabolism,
HSP7C_MOUSE	heat shock protein 8(Hspa8)	-0.73	Spliceosome, MAPK signaling pathway, Protein processing in endoplasmic reticulum, Endocytosis, Antigen processing and presentation, Estrogen signaling pathway, Legionellosis, Toxoplasmosis, Measles, Influenza A,
HS90A_MOUSE	heat shock protein 90, alpha (cytosolic), class A member 1(Hsp90aa1)	-0.63	Protein processing in endoplasmic reticulum, PI3K-Akt signaling pathway, Antigen processing and presentation, NOD-like receptor signaling pathway
HPRT_MOUSE	hypoxanthine guanine phosphoribosyl transferase(Hprt)	-0.67	Purine metabolism, Drug metabolism - other enzymes, Metabolic pathways,
PDXK_MOUSE	pyridoxal (pyridoxine, vitamin B6) kinase(Pdxk)	-0.78	Vitamin B6 metabolism, Metabolic pathways,
KPYM_MOUSE	pyruvate kinase, muscle(Pkm)	-0.67	Glycolysis / Gluconeogenesis, Purine metabolism, Pyruvate metabolism, Metabolic pathways, Biosynthesis of antibiotics, Carbon metabolism, Biosynthesis of amino acids,

A1AT1_MOUSE	serine (or cysteine) peptidase inhibitor, clade A, member 1A(Serpina1a)	-0.64	Complement and coagulation cascades,
A1AT2_MOUSE	serine (or cysteine) preptidase inhibitor, clade A, member 1B(Serpina1b)	-0.64	Complement and coagulation cascades,
SYSC_MOUSE	seryl-aminoacyl-tRNA synthetase(Sars)	-0.69	Aminoacyl-tRNA biosynthesis,
THOP1_MOUSE	thimet oligopeptidase 1(Thop1)	-0.78	Renin-angiotensin system, African trypanosomiasis,
TKT_MOUSE	transketolase(Tkt)	-0.83	Pentose phosphate pathway, Metabolic pathways, Biosynthesis of antibiotics, Carbon metabolism, Biosynthesis of amino acids,

4. Endothelial TJ proteins disorganized in brains of *ANXA2*-KO mice after lethal SFGR infections.

The overall functional enrichment analysis supports our hypothesis that deletion of ANXA2 affects the cell-cell junction structure during the rickettsial infection. However, LC/MS showed that the expression level of TJ protein ZO-1 in the brain was similar between infected *ANXA2*-KO and infected WT mice. We postulated that strutures of TJ might be disorganized instead of downregulation of the expression levels.

Occludin, directly interacted with ZO-1, is an important transmembrane protein integral to TJs[88]. To investigate the structure of TJs, we applied IF assay to the brain tissue to examine ZO-1 and occludin. Remarkably, in all five *ANXA2*-KO mice, dramatic disruption and disorganization of ZO-1 and occludin were detected after D5 p.i. (**Fig. 8A**). Interestingly, occludin disorganization was also observed in the livers of these *ANXA2*-KO mice on day 5 p.i. (**Fig. 8B**). AJ protein VE-cadherins were also investigated. Animals in both WT and *ANXA2*-KO groups exhibited similar disintegrated structures of VE-cadherin in response to *R. australis* infection on day 5 p.i. (**Fig. 8C**).

5. **CMHs and disorganized EC TJs in ANXA2-KO mice subjected to Ebola virus infection.**

Similar to rickettsia, Ebola virus is known to attack the endothelial cells and a severe vascular leakage syndrome is a major complication during Ebola infection[64-69]. We investigated whether the *ANXA2* deletion-dependent CMHs was also present in Ebola virus infection via retrospective histology examination of brain tissue samples from WT (n=5) or *ANXA2*-KO (n=5) mice

challenged by a mouse-adapted strain of Ebola Zaire virus (50 plaque-forming unit by the intraperitoneal route[89]). A 20% cumulative survival was observed in *ANXA2*-KO mice 12 days p.i., compared with an 80% cumulative survival in the group of WT mice at the same time (p=0.08, Log-rank test) (**Supplemental Fig. 2**). IF assay of Ebola virus in the liver, brain and lung tissues showed no difference between WT and *ANXA2*-KO mice on day 7-12 p.i. (**Fig. 9A**).

Similarly, CMHs was detected in H&E staining in all *ANXA2*-KO mice (**Fig. 9C-E**), but not in WT mice (**Fig. 9B**) during 7-12 days p.i.. Furthermore, disorganized TJ protein ZO-1 and occludin were also present in brain tissue from *ANXA2*-KO, but not WT mice (**Fig. 9F**) infected with same dose of Ebola virus intraperitoneally. Furthermore, dramatic disruption and disorganization of occludin were also observed in the livers of *ANXA2*-KO mice post Ebola virus infection (**Fig. 9G**).

Collectively, these data suggest the detriments to the TJ structures as an underlying mechanism of the CMHs observed in *ANXA2*-KO mice post-*R. australis* or Ebola virus infections.

6. Other considerations

An earlier study reported that the deletion of ANXA2 rendered mice susceptible to chemically-induced carotid arterial thrombosis[90]. To determine the possible involvement of thrombus formation, which is associated with EC injury[91], in cerebral microhemorrhage, we examine all H&E staining and no thrombus was visualized.

We previously showed that the exchange protein directly activated by cAMP (EPAC) plays a critical role during SFGR infections[80] and that EPAC regulates ANXA2-mediated vascular fibrinolysis[92]. Given the regulatory role of EPAC on ANXA2, we retrospectively reviewed archival H&E-stained brain sections of EPAC1-deficient mice[80, 92] infected with an ordinary lethal dose of SFGR, but no histological evidence of CMHs was found, suggesting EPAC is not associated with CMHs during infections.

Discussion

In this study, we report a novel finding that *ANXA2*-KO mice are more susceptible to rickettsia- or Ebola virus-induced CMHs, underlying mechanisms relevant to endothelial TJs-based BBB dysfunction. Furthermore, we performed a proteomic analysis on the whole brain lysate and isolated endosomes using LC/MS. The obtained list of differentially expressed proteins was subjected to function enrichment analysis, combining GO term and KEGG pathway.

Whole-brain lysate proteomic functional group

Cell-cell junction

BBB properties are primarily determined by BMEC AJs and TJs. Cell-cell AJ junction offers contracting force to bridge adjacent ECs via cadherins and nectins [93]. It physically interacts with TJs and indirectly links to TJ via actin-associated proteins[88, 93]. It is reported that AXNA2 is directly associated with AJ stability. The depletion of ANXA2 dissociates VE-cadherin from AJ[73]. The identified proteins associated with AJs include myosin heavy polypeptide 9 (non-muscle), septins, tyrosine 3-monooxygenase/tryptophan 5-monooxygenase activation protein, HSP90α (cytosolic), aldolase A, enolase 1, heat shock protein 5.These proteins are not direct structural proteins of the AJ such as VE-cadherin and beta-catenin but closely related to AJ assembly and stability. For example, inhibition of HSP90α is capable of attenuate the reduced VE-cadherin and beta catenin level induced by thrombin, LPS, VEGF, or TGF-β1, which all are known to increase endothelial permeability [94-96]. It is also suggested that HSP90α is a downstream effector of RhoA signaling, which is mediated by LPS[96]. Our data shows that HSP90α level was increased 9.4-fold in *ANXA2*-KO brain compared to WT post rickettsia infection. Elevated levels of HSP90α could lead to the instability of the AJ in the presence of LPS[97]. The association of HSP90α and ANXA2 has not been fully understood. There is only one published study supporting the association, showing that high glucose increases *ANXA2* expression in ECs and enhances the association of HSP90α and ANXA2 in both ECs and rat aorta[98]. The functional interaction between ANXA2 and hsp90 in the context of pathogen infection is largely unknown.

Stress fiber

Stress fiber is formed by contractile actin filament bundle and a variety of proteins responsible for actin stabilization including septins, α-actin, tropomyosin, Rho-associated protein kinase (ROCK), fascin, and myosin 2, etc.[99]. It is formed in the cells in response to the environmental mechanical stress, therefore only a subset of cells in the body can form stress fiber, such as ECs in the presence of fluid shear stress. Cells cultured on stiff substrate form stress fiber whereas those on the soft substrate have much less fiber. Physiologically, stress fiber is important for cell adhesion, mechanotransduction and AJ maturation[99-101]. Stress fiber plays a positive role in AJ maturation, but it is not always the case in the pathological environment. Such phenomenon is also seen in VEGF- and activated-neutrophil-treated ECs[102, 103].

Our data report four DE proteins in the stress fiber category: septin 5, septin 7, tropomyosin 1 and tropomyosin 3. Three out of the four proteins were increased in *ANXA2*-KO group. The

association of ANXA2 to stress fiber formation is elusive. In BHK-IR cells, insulin-mediated loss of stress fiber and resulting cell detachment depend on the presence of AXNA2 and its tyrosine phosphorylation state[74]. Silencing *ANXA2* with siRNA in MOI Muller cells directly leads to the accumulation of stress fiber[70].

Isolated endosome function group

Cell-cell junctions

AJ is a significantly enriched functional group. Ten proteins were found in this category. Endocytosis is known to mediate the stability of AJ[104]. Based on structural analysis using IF and drug intervention, Georgiou et al, suggested that impaired endocytosis leads to AJ instability[104]. AXNA2 is involved in the formation of early endosomes. AXNA2 depletion results in morphological changes in endosomes and alters their distribution[73]. Our proteomic data analyzing the protein difference between WT and *ANXA2*-KO mice upon rickettsial infection identified 10 proteins associated with AJ in the brain endosomal compartment. Interestingly, cadherin complex protein cadherin 2 and talin 1 were upregulated in *ANXA2*-KO after infections. Cadherin 2 is a direct structural protein of AJ, and it is involved in pericyte-EC adhesion, which is critical for the integrity of the BBB. Focal injection of antibody against cadherin-2 is sufficient to induce intracerebral hemorrhage[105]. The biological significance of cadherin-2 upregulation in the endosomal compartment is unknown. It has been shown, however, that cadherin-2 and other several other junction-associated proteins were subjected to rapid endocytosis in a drug-induced disruption of cell-cell contact model [106]. Talin 1 is a well-known AJ-associated protein located at the cytoplasmic side to the AJ[107]. Endosomal talin has been shown to regulate the function of endosomal integrin[108].

MHC II protein complex binding and stress response

Three major players are found in MHC II protein complex binding: HSP90α, heat shock protein 8 (HSPa8), and pyruvate kinase. HSP90α is noteworthy. In *ANXA2*-KO mice, it was drastically enriched in whole-brain but decreased in the endosomal compartment, indicating a reduced protein turnover rate or degradation. Given the direct association of ANXA2 and endocytosis, ANXA2 may be an upstream regulator of HSP90α responsible for its recycling upon stimulation. HSP90α is involved in the disruption of BBB function post cerebral ischemic stroke. Inhibition of HSP90α with ATP competitive inhibitor results in reduced activity of metalloproteinase 9 (MMP9), which plays an important role in BBB dysfunction, and rescues TJ

protein expression abnormality[109]. HSP90α is also associated with inflammation induced by LPS[110]. It has been shown that the involvement of HSP90α is associated with PI3K and NF-κB pathways[111]. Therefore, a possible mechanism explaining the increased susceptibility of *ANXA2*-KO to *R.australis*-induced CMH is that ANXA2 depletion causes reduced degradation of HSP90α, which destabilizes the cell-cell junction and increases the hyperpermeability of BBB. So far AXNA2 is known to interact with HSP90α and such interaction is increased in the presence of high glucose[98], yet the role of HSP90α-AXNA2 interaction in bacterial infection is unknown. Further *in vitro* experiment is needed to confirm this mechanism.

HSPa8 is a noncanonical member of the heat shock protein 70 family[112]. The majority of HSPa8 resides in the cytosol and nucleus, but upon stimulation, it also translocates to the plasma membrane or exosome, contributing to antigen presentation via MHC II to CD4 T cells, clathrin-mediated vesicles transport, and chaperone-dependent autophagy[112, 113]. In our data, similar to HSP90α, HSPa8 was found to be reduced in the endosomal compartment in *ANXA2*-KO group, whereas it was upregulated in the whole brain lysate (one-fold). However, the biological role of the association between AXNA2 and HSPa8 is unknown.

HSP90α, HSP8 and mitogen-activated protein kinase kinase 4(Map2k4) comprise another functional group, stress response. Map2k4 is a direct activator of c-jun activation protein kinase (JNK) [114]. Map2k4 was enriched in the endosomal compartment in *ANXA2*-KO mice brain compared to WT. Interestingly, it has been reported that *ANXA2* knockdown by shRNA enhances the activation of JNK and p38 in response to oxidative stress[115].

Conclusion

Our data suggest that 1) ANXA2 per se does not affect the proliferation of *R. australis* or Ebola virus. 2) Also, *ANXA2*-KO does not significantly affect the survival of the mice post-acute *R. australis*. 3) Inflammatory cytokines TNFα and IFNγ are not affected by ANXA2 knock out. 4) ANXA2 is required for stabilizing BBB, especially endothelial TJs during rickettsia and Ebola virus infections. 5) The most relevant functional groups that could be intertwined with the contingent function of ANXA2 are cell-cell junction, stress fiber, and MHC II binding complex, shown by functional enrichment analysis combining the whole-brain lysate and isolated endosome proteome.

Among all the DE proteins we have identified in this study, HSP90α is the most noteworthy because it was present in multiple vascular integrity relevant functional enriched groups. HSP90α

is closely related to endothelial hyperpermeability[94]. In our proteomic data, it is upregulated in the whole brain lysate compartment while downregulated in the isolated endosome, indicating that its endocytosis dependent degradation might be impaired.

In conclusion, this is the first report that correlates the special role of ANXA2 and CMHs in the context of rickettsial and Ebola virus infections. Further experiments on the *in vitro* multi-cell co-culture BBB system are necessary to delineate underlying mechanism(s).

Materials and methods

Biologic containment.

Infectious material and animals were handled in maximum-containment biosafety level 3 (for *R. australis*) and 4 (for Ebola virus) facilities at the Galveston Nationa Laboratory (GNL), University Texas Medical Branch at Galveston.

Ethics statement

All animal protocols were approved by the Institutional Animal Care and Use Committee of the University of Texas Medical Branch (protocol # 1702018 and protocol # 9505045G). The animal studies were carried out in strict accordance with the recommendations in the Guide for the Care and Use of Laboratory Animals of the National Institutes of Health, USA.

SFGR mouse infection model[80, 116]

ANXA2-KO on C57BL/6 background and C57BL/6 mice were used in this study. Animals (15 WT and 14 *ANXA2*-KO mice) were inoculated with 2LD50 dose (2×10^6 pfu per mouse) of *R. australis* via tail vein injection and observed daily. All procedures followed the approved IACUC protocol. Signs of ruffled fur, hunched posture, labored breathing and closed eyelids were identified as lethal illness (41, 42). The animals were observed for 10 days when most of the animals were all in lethal illness state. For time-dependent pathological study, mice were inoculated with 2 LD50 dose of *R. australis* and euthanized at day 2, 4, 5 post-infection (n=5 for each time point). For mass spectrometry experiments, animals (WT or *ANXA2*-KO) were euthanized at 5 days p.i. and the brain samples were collected and digested into protein lysate for downstream analysis. The time point was selected for LC/MS because this was when mice started to showing up lethal illness.

Ebola virus mouse infection model[89]

To observe the effect of mice with *ANXA2*-KO compared to WT on Ebola hemorrhagic disease, C57BL6 6-12 week wild type (n=5) and *ANXA2*-KO mice were inoculated intraperitoneally with

50 plaque-forming unit of mouse-adapted strain of Ebola Zaire (Mayinga) virus (provided by Thomas Ksiazek) in 200 uL of PBS. All procedures followed approved IACUC protocol. Mice were monitored multiple times daily for signs of illness and mortality p.i. Daily observations included evaluation of mice for clinical symptoms such as reduced grooming, ruffled fur, hunched posture, subdued response to stimulation, nasal discharge, and bleeding. Tissues and carcasses were collected for downstream assays.

Sample collection

Blood samples were collected via orbital sinus and serum was obtained after centrifuge and discarding the cellular content of the blood. Complete necropsies were performed on all mice to obtain the organs. For immunohistochemistry or H&E staining, organs were fixed in a 4% (vol/vol) formaldehyde. For mass spectrometry, brain tissues were lysed in protein lysing buffer with proteinase inhibitor and phosphatase inhibitor. Endosome isolation was perform using Minute^{TM} endosome and cell fraction kit.

IF and H&E staining

The fixed samples were subjected to H&E staining or immunofluorescence (IF) with an antibody against the protein of interest. For IF studies on mouse tissue with mouse antibody, tissue sections were blocked with unconjugated AffiniPure Fab fragment goat anti-mouse IgG (H+L) for 1 hour at room temperature first before incubation with antibodies against ZO-1, occludin, SFG rickettsiae, or Ebola virus overnight at 4 °C, followed by secondary antibody AlexaFluor 594 goat anti-mouse or AlexaFluor 488 goat anti-rabbit antibodies. Before mounting to the cover slide, the tissue sections were stained with DAPI. Normal rabbit and mouse IgGs were used as negative reagent controls (**Supplemental Fig. 1C**). Fluorescent images were taken and analyzed with an Olympus BX51 microscope.

DNA extraction and rt-qPCR

To quantify the rickettsia loading in the brain tissue, the DNeasy tissue kit (Qiagen, CA, 69506) was used to quantify DNA rickettsial DNA. Briefly, the brain samples were minced into pieces, and subjected to lysis buffer and proteinase k digestion for 10 minutes in 56 degrees Celsius; then DNA was precipitated in ethanol and purified using washing buffer. The purified DNA samples were stored in storage buffer in -20 C^{o} . PCR was performed using the protocol as previously described [117]. Rickettsia-specific citrate synthase (CS) gene (gltA) was used as the target for

rickettsia detection (gltA forward: GAGAGAAAATTATATCCAAATGTTGAT; gltA reverse, AGGGTCTTCGTGCATTTCTT)[117].

ELISA

Plasma samples collected from *ANXA2*-KO and WT mice were used for ELISA to detect TNFα (Qantikine ELISA, MTA00B) and IFNγ (Qantikine ELISA, MIF00). Standard curves were performed using the standard proteins according to the protocol provided in the ELISA kits. The ELISA plates were detected at 450nm.

LC-MS/MS

Proteins were acetone-precipitated and cleaned with 1 ml of ice-cold wash solution (tri-*n*-butyl phosphate/acetone/methanol (1:12:1 by volume) for 90 minutes and then centrifuged at 2800g for 15 minutes at 4°C. The supernatant was removed and 1 ml ice-cold tri-*n*-butyl phosphate was added and incubated at 4°C for 15 minutes and then centrifuged at 2800g for 15 minutes at 4°C. The supernatant was discarded and 1 ml ice-cold acetone was added and incubated at 4°C for 15 minutes and then centrifuged at 2800g for 15 minutes at 4°C. The supernatant was discarded and 1 ml ice-cold methanol was added and incubated at 4°C for 15 minutes and then centrifuged at 2800g for 15 minutes at 4°C. 50ug of protein was solubilized with 5% SDS, 50 mM TEAB, pH 7.55, in the final volume of 25 uL. The sample was then centrifuged at 17,000g for 10 minutes for debris removal. Proteins were reduced by making the solution 20mM TCEP (Thermo, #77720) and incubated at 65°C for 30 minutes. The sample was cooled to room temperature. After 1 uL of 0.5 M iodoacetamide acid was added, the sample was allowed to react for 20 minutes in the dark. 2.75 ul of 12% phosphoric acid was added to the protein solution. 165uL of binding buffer (90% Methanol, 100mM TEAB final; pH 7.1) was then added to the solution. The resulting solution was loaded onto a S-Trap spin column (protifi.com) and passed through the column by a benchtop centrifuge (30-second spin at 4,000g). The spin column was washed with 400uL of binding buffer and centrifuged. The wash was repeated two more times. Trypsin was added to the protein mixture in a ratio of 1:25 in 50mM TEAB, pH=8, and incubated at 37°C for 4 hours. Peptides were eluted with 80 uL of 50 mM TEAB, followed by 80 uL of 0.2% formic acid, and finally 80 uL of 50% acetonitrile, 0.2% formic acid. The combined peptide solution was then dried in a speed vac and resuspended in 2% acetonitrile, 0.1% formic acid, 97.9% water and placed in an autosampler vial.

NanoLC MS/MS Analysis.

Instrument performance was verified by analyzing a standard peptide mix and a complex protein digest (HeLa) before the sample set was run between each experimental block and at the end of the experiment. The HeLa data files were analyzed in order to confirm that instrument performance remained consistent throughout the experiment. Peptide mixtures from digested brain tissue were analyzed by nanoflow liquid chromatography-tandem mass spectrometry (nanoLC-MS/MS) using a nano-LC chromatography system (UltiMate 3000 RSLCnano, Dionex), coupled on-line to a Thermo Orbitrap Fusion mass spectrometer (Thermo Fisher Scientific, San Jose, CA) through a nanospray ion source (Thermo Scientific). A trap and elute method was used. The trap column is a C18 PepMap100 (300um X 5mm, 5um particle size) from ThermoScientific. The analytical columns is an Acclaim PepMap 100 (75um X 25 cm) from (Thermo Scientific). After equilibrating the column in 98% solvent A (0.1% formic acid in water) and 2% solvent B (0.1% formic acid in acetonitrile (ACN)), the samples (1 µL in solvent A) were injected onto the trap column and subsequently eluted (400 nL/min) by gradient elution onto the C18 column as follows: isocratic at 2% B, 0-5 minutes; 2% to 32% B, 5-100 minutes; 32% to 50% B, 100-108 minutes; 50% to 90% B, 108-109 minutes; isocratic at 90% B, 109-114 minutes; 90% to 2%, 114-115 minutes; and isocratic at 2% B, till 130 minutes.

All LC-MS/MS data were acquired using XCalibur, version 2.1.0 (Thermo Fisher Scientific) in positive ion mode using a top speed data-dependent acquisition (DDA) method with a 3 sec cycle time. The survey scans (*m/z* 350-1500) were acquired in the Orbitrap at 120,000 resolution (at *m/z* = 400) in profile mode, with a maximum injection time of 50 msec and an AGC target of 400,000 ions. The S-lens RF level was set to 60. Isolation was performed in the quadrupole with a 1.6 Da isolation window, and CID MS/MS acquisition was performed in profile mode using rapid scan rate with detection in the orbitrap (res: 35,000), with the following settings: parent threshold = 5,000; collision energy = 35%; maximum injection time 100 msec; AGC target 500,000 ions. Monoisotopic precursor selection (MIPS) and charge state filtering were on, with charge states 2-6 included. Dynamic exclusion was used to remove selected precursor ions, with a +/- 10 ppm mass tolerance, for 60 sec after acquisition of one MS/MS spectrum.

Database Searching**.** Tandem mass spectra were extracted and charge state deconvoluted by Proteome Discoverer (Thermo Fisher, version 1.4.1.14). Deisotoping was not performed. All MS/MS spectra were searched using Sequest. Searches were performed with a parent ion tolerance of 5 ppm and a fragment ion tolerance of 0.60 Da. Trypsin was specified as the enzyme, allowing

for two missed cleavages. Fixed modification of carbamidomethyl (C) and variable modifications of oxidation (M) and deamidation of asparagine and glutamine, were specified in Sequest. Scaffold (version Scaffold_4.8.7, Proteome Software Inc., Portland, OR) was used to validate MS/MS-based peptide and protein identifications. Peptide identifications were accepted if they could be established at greater than 95.0% probability. Peptide Probabilities from X! Tandem and Sequest were assigned by the Scaffold Local FDR algorithm. Peptide Probabilities were assigned by the Peptide Prophet algorithm [118] with Scaffold delta-mass correction. Protein identifications were accepted if they could be established at greater than 95.0% probability and contained at least 2 identified peptides. Protein probabilities were assigned by the Protein Prophet algorithm [118]. Proteins that contained similar peptides and could not be differentiated based on MS/MS analysis alone were grouped to satisfy the principles of parsimony.

Functional enrichment analysis

Raw mass spectrometry data was filtered to rule out low abundance protein. Specifically, proteins that are included in the analysis must have at least 4 total spectra count. A list of differentially expressed proteins was obtained by comparing the -spectral counts between *ANXA2*-KO and WT groups and calculating the fold change. Proteins with a fold change greater than or equal to 2 were considered upregulated; protein with fold change less than or equal to -0.6 were considered down-regulated. Selected DE proteins are listed in Table 1-4. Next, the DE proteins were further annotated using The Database for Annotation, Visualization and Integrated Discovery (DAVID) v6.8, which is also capable of doing functional enrichment analysis. Functional enrichment analysis helps us better correlate the molecular patterns with the gross pathology we have observed in the animal model. GO term and KEGG pathways were used to categorize the DE proteins (Figure 1). The Biological Networks Gene Ontology tool (BiNGO) [119] was used to perform the network analysis, which provides a direct structural visualization of the functional enriched groups. Protein-protein interaction (PPI) network was performed using Cytoscape GeneMania[120].

Acknowledgment

We gratefully acknowledge Dr. Katherin Hajjar for providing the *ANXA2*-KO breeders. We gratefully acknowledge Drs. David Walker and Gerk Volker for reagent support. We gratefully acknowledge Dr. Donald Bouyer for BSL3 facility support. We thank Drs. Shangyi Yu, Xiang Li, Ben Zhang, and Junyin Zheng for technical support. This work was supported by NIH grant

R01AI121012 (B.G.) and R21AI137785 (B.G.). The funders have no role in the study design, data collection and analysis, decision to publish, or preparation of the manuscript.

Reference

1. Greenberg SM, Vernooij MW, Cordonnier C, Viswanathan A, Al-Shahi Salman R, Warach S, et al. Cerebral microbleeds: a guide to detection and interpretation. Lancet Neurol. 2009;8(2):165-74. doi: 10.1016/S1474-4422(09)70013-4. PubMed PMID: 19161908; PubMed Central PMCID: PMCPMC3414436.
2. Ungvari Z, Tarantini S, Kirkpatrick AC, Csiszar A, Prodan CI. Cerebral microhemorrhages: mechanisms, consequences, and prevention. Am J Physiol Heart Circ Physiol. 2017;312(6):H1128-H43. Epub 2017/03/17. doi: 10.1152/ajpheart.00780.2016. PubMed PMID: 28314762; PubMed Central PMCID: PMCPMC5495931.
3. Schlunk F, Böhm M, Boulouis G, Qin T, Arbel M, Tamim I, et al. Secondary Bleeding During Acute Experimental Intracerebral Hemorrhage. Stroke. 2019;50(5):1210-5. doi: 10.1161/STROKEAHA.118.021732. PubMed PMID: 31009358; PubMed Central PMCID: PMCPMC6478448.
4. Fisher M, French S, Ji P, Kim RC. Cerebral microbleeds in the elderly: a pathological analysis. Stroke. 2010;41(12):2782-5. Epub 2010/10/28. doi: 10.1161/STROKEAHA.110.593657. PubMed PMID: 21030702; PubMed Central PMCID: PMCPMC3079284.
5. Koennecke HC. Cerebral microbleeds on MRI: prevalence, associations, and potential clinical implications. Neurology. 2006;66(2):165-71. doi: 10.1212/01.wnl.0000194266.55694.1e. PubMed PMID: 16434647.
6. Chien LN, Chi NF, Hu CJ, Chiou HY. Central nervous system infections and stroke -- a population-based analysis. Acta Neurol Scand. 2013;128(4):241-8. Epub 2013/04/01. doi: 10.1111/ane.12116. PubMed PMID: 23550811.
7. Siler DA, Berlow YA, Kukino A, Davis CM, Nelson JW, Grafe MR, et al. Soluble Epoxide Hydrolase in Hydrocephalus, Cerebral Edema, and Vascular Inflammation After Subarachnoid Hemorrhage. Stroke. 2015;46(7):1916-22. Epub 2015/05/19. doi: 10.1161/STROKEAHA.114.008560. PubMed PMID: 25991416; PubMed Central PMCID: PMCPMC4480190.
8. Benakis C, Garcia-Bonilla L, Iadecola C, Anrather J. The role of microglia and myeloid immune cells in acute cerebral ischemia. Front Cell Neurosci. 2014;8:461. Epub 2015/01/14. doi: 10.3389/fncel.2014.00461. PubMed PMID: 25642168; PubMed Central PMCID: PMCPMC4294142.
9. Baltan S. Ischemic injury to white matter: an age-dependent process. Neuroscientist. 2009;15(2):126-33. doi: 10.1177/1073858408324788. PubMed PMID: 19307420.
10. Guell K, Bix GJ. Brain endothelial cell specific integrins and ischemic stroke. Expert Rev Neurother. 2014;14(11):1287-92. Epub 2014/09/29. doi: 10.1586/14737175.2014.964210. PubMed PMID: 25262658.
11. Yang C, Hawkins KE, Doré S, Candelario-Jalil E. Neuroinflammatory mechanisms of blood-brain barrier damage in ischemic stroke. Am J Physiol Cell Physiol. 2019;316(2):C135-C53. Epub 2018/10/31. doi: 10.1152/ajpcell.00136.2018. PubMed PMID: 30379577; PubMed Central PMCID: PMCPMC6397344.
12. Wolf MS, Bayır H, Kochanek PM, Clark RSB. The role of autophagy in acute brain injury: A state of flux? Neurobiol Dis. 2019;122:9-15. Epub 2018/04/26. doi: 10.1016/j.nbd.2018.04.018. PubMed PMID: 29704549; PubMed Central PMCID: PMCPMC6203674.
13. Tomura S, de Rivero Vaccari JP, Keane RW, Bramlett HM, Dietrich WD. Effects of therapeutic hypothermia on inflammasome signaling after traumatic brain injury. J Cereb Blood Flow Metab. 2012;32(10):1939-47. Epub 2012/07/11. doi: 10.1038/jcbfm.2012.99. PubMed PMID: 22781337; PubMed Central PMCID: PMCPMC3463887.

14. Hsu M, Rayasam A, Kijak JA, Choi YH, Harding JS, Marcus SA, et al. Neuroinflammation-induced lymphangiogenesis near the cribriform plate contributes to drainage of CNS-derived antigens and immune cells. Nat Commun. 2019;10(1):229. Epub 2019/01/16. doi: 10.1038/s41467-018-08163-0. PubMed PMID: 30651548; PubMed Central PMCID: PMCPMC6335416.
15. Kotoda M, Furukawa H, Miyamoto T, Korai M, Shikata F, Kuwabara A, et al. Role of Myeloid Lineage Cell Autophagy in Ischemic Brain Injury. Stroke. 2018;49(6):1488-95. Epub 2018/05/10. doi: 10.1161/STROKEAHA.117.018637. PubMed PMID: 29748423; PubMed Central PMCID: PMCPMC5970995.
16. DeKosky ST, Abrahamson EE, Ciallella JR, Paljug WR, Wisniewski SR, Clark RS, et al. Association of increased cortical soluble abeta42 levels with diffuse plaques after severe brain injury in humans. Arch Neurol. 2007;64(4):541-4. doi: 10.1001/archneur.64.4.541. PubMed PMID: 17420316.
17. Nasr IW, Chun Y, Kannan S. Neuroimmune responses in the developing brain following traumatic brain injury. Exp Neurol. 2019;320:112957. Epub 2019/05/17. doi: 10.1016/j.expneurol.2019.112957. PubMed PMID: 31108085.
18. Su EJ, Lawrence DA. α2 Antiplasmin and microvascular thrombosis in ischemic stroke. Arterioscler Thromb Vasc Biol. 2014;34(12):2522-3. doi: 10.1161/ATVBAHA.114.304616. PubMed PMID: 25411105.
19. Sabirzhanov B, Faden AI, Aubrecht T, Henry R, Glaser E, Stoica BA. MicroRNA-711-Induced Downregulation of Angiopoietin-1 Mediates Neuronal Cell Death. J Neurotrauma. 2018;35(20):2462-81. Epub 2018/07/10. doi: 10.1089/neu.2017.5572. PubMed PMID: 29774773; PubMed Central PMCID: PMCPMC6196751.
20. Yi JH, Park SW, Kapadia R, Vemuganti R. Role of transcription factors in mediating post-ischemic cerebral inflammation and brain damage. Neurochem Int. 2007;50(7-8):1014-27. Epub 2007/05/03. doi: 10.1016/j.neuint.2007.04.019. PubMed PMID: 17532542; PubMed Central PMCID: PMCPMC2040388.
21. Ding Y, Flores J, Klebe D, Li P, McBride DW, Tang J, et al. Annexin A1 attenuates neuroinflammation through FPR2/p38/COX-2 pathway after intracerebral hemorrhage in male mice. J Neurosci Res. 2019. Epub 2019/06/03. doi: 10.1002/jnr.24478. PubMed PMID: 31157469.
22. Askenase MH, Sansing LH. Stages of the Inflammatory Response in Pathology and Tissue Repair after Intracerebral Hemorrhage. Semin Neurol. 2016;36(3):288-97. Epub 2016/05/23. doi: 10.1055/s-0036-1582132. PubMed PMID: 27214704; PubMed Central PMCID: PMCPMC4956485.
23. Han X, Lan X, Li Q, Gao Y, Zhu W, Cheng T, et al. Inhibition of prostaglandin E2 receptor EP3 mitigates thrombin-induced brain injury. J Cereb Blood Flow Metab. 2016;36(6):1059-74. Epub 2015/10/02. doi: 10.1177/0271678X15606462. PubMed PMID: 26661165; PubMed Central PMCID: PMCPMC4908617.
24. Bonsack F, Alleyne CH, Sukumari-Ramesh S. Augmented expression of TSPO after intracerebral hemorrhage: a role in inflammation? J Neuroinflammation. 2016;13(1):151. Epub 2016/06/17. doi: 10.1186/s12974-016-0619-2. PubMed PMID: 27315802; PubMed Central PMCID: PMCPMC4912814.
25. Jickling GC, Ander BP, Shroff N, Orantia M, Stamova B, Dykstra-Aiello C, et al. Leukocyte response is regulated by microRNA let7i in patients with acute ischemic stroke. Neurology. 2016;87(21):2198-205. Epub 2016/10/26. doi: 10.1212/WNL.0000000000003354. PubMed PMID: 27784773; PubMed Central PMCID: PMCPMC5123554.
26. Chen-Roetling J, Cao Y, Peng D, Regan RF. Rapid loss of perihematomal cell viability in the collagenase intracerebral hemorrhage model. Brain Res. 2019;1711:91-6. Epub 2019/01/10. doi: 10.1016/j.brainres.2019.01.014. PubMed PMID: 30639124; PubMed Central PMCID: PMCPMC6519080.
27. Huggins MA, Johnson HL, Jin F, N Songo A, Hanson LM, LaFrance SJ, et al. Perforin Expression by CD8 T Cells Is Sufficient To Cause Fatal Brain Edema during Experimental Cerebral Malaria. Infect Immun. 2017;85(5). Epub 2017/04/21. doi: 10.1128/IAI.00985-16. PubMed PMID: 28264905; PubMed Central PMCID: PMCPMC5400849.

28. Willenbring RC, Jin F, Hinton DJ, Hansen M, Choi DS, Pavelko KD, et al. Modulatory effects of perforin gene dosage on pathogen-associated blood-brain barrier (BBB) disruption. J Neuroinflammation. 2016;13(1):222. Epub 2016/08/31. doi: 10.1186/s12974-016-0673-9. PubMed PMID: 27576583; PubMed Central PMCID: PMCPMC5006384.
29. Yang D, Sun YY, Lin X, Baumann JM, Dunn RS, Lindquist DM, et al. Intranasal delivery of cell-penetrating anti-NF-κB peptides (Tat-NBD) alleviates infection-sensitized hypoxic-ischemic brain injury. Exp Neurol. 2013;247:447-55. Epub 2013/01/23. doi: 10.1016/j.expneurol.2013.01.015. PubMed PMID: 23353638; PubMed Central PMCID: PMCPMC4064308.
30. Aronowski J, Roy-O'Reilly MA. Neutrophils, the Felons of the Brain. Stroke. 2019;50(3):e42-e3. doi: 10.1161/STROKEAHA.118.021563. PubMed PMID: 30674235; PubMed Central PMCID: PMCPMC6544162.
31. Manousakis G, Jensen MB, Chacon MR, Sattin JA, Levine RL. The interface between stroke and infectious disease: infectious diseases leading to stroke and infections complicating stroke. Curr Neurol Neurosci Rep. 2009;9(1):28-34. PubMed PMID: 19080750.
32. Nakano K, Hokamura K, Taniguchi N, Wada K, Kudo C, Nomura R, et al. The collagen-binding protein of Streptococcus mutans is involved in haemorrhagic stroke. Nat Commun. 2011;2:485. Epub 2011/09/27. doi: 10.1038/ncomms1491. PubMed PMID: 21952219; PubMed Central PMCID: PMCPMC3220351.
33. Hyacinth HI, Sugihara CL, Spencer TL, Archer DR, Shih AY. Higher prevalence of spontaneous cerebral vasculopathy and cerebral infarcts in a mouse model of sickle cell disease. J Cereb Blood Flow Metab. 2019;39(2):342-51. Epub 2017/09/19. doi: 10.1177/0271678X17732275. PubMed PMID: 28925802; PubMed Central PMCID: PMCPMC6365608.
34. Corrêa DG, Cruz Júnior LC, Bahia PR, Gasparetto EL. Intracerebral microbleeds in sepsis: susceptibility-weighted MR imaging findings. Arq Neuropsiquiatr. 2012;70(11):903-4. PubMed PMID: 23175208.
35. Amaro M, Bacellar F, França A. Report of eight cases of fatal and severe Mediterranean spotted fever in Portugal. Ann N Y Acad Sci. 2003;990:331-43. PubMed PMID: 12860647.
36. Horney LF, Walker DH. Meningoencephalitis as a major manifestation of Rocky Mountain spotted fever. South Med J. 1988;81(7):915-8. PubMed PMID: 3393952.
37. Garc Ía-Baena C, Cárdenas MF, Ramón JF. Cerebral haemorrhage as a clinical manifestation of human ehrlichiosis. BMJ Case Rep. 2017;2017. Epub 2017/07/27. doi: 10.1136/bcr-2016-219054. PubMed PMID: 28751428.
38. Bonney S, Seitz S, Ryan CA, Jones KL, Clarke P, Tyler KL, et al. Gamma Interferon Alters Junctional Integrity via Rho Kinase, Resulting in Blood-Brain Barrier Leakage in Experimental Viral Encephalitis. MBio. 2019;10(4). Epub 2019/08/06. doi: 10.1128/mBio.01675-19. PubMed PMID: 31387911; PubMed Central PMCID: PMCPMC6686045.
39. Sumbria RK, Grigoryan MM, Vasilevko V, Krasieva TB, Scadeng M, Dvornikova AK, et al. A murine model of inflammation-induced cerebral microbleeds. J Neuroinflammation. 2016;13(1):218. Epub 2016/08/30. doi: 10.1186/s12974-016-0693-5. PubMed PMID: 27577728; PubMed Central PMCID: PMCPMC5006574.
40. Joó F. The blood-brain barrier. Nature. 1987;329(6136):208. doi: 10.1038/329208b0. PubMed PMID: 3627266.
41. Zhao Z, Nelson AR, Betsholtz C, Zlokovic BV. Establishment and Dysfunction of the Blood-Brain Barrier. Cell. 2015;163(5):1064-78. doi: 10.1016/j.cell.2015.10.067. PubMed PMID: 26590417; PubMed Central PMCID: PMCPMC4655822.
42. Aydin F, Rosenblum WI, Povlishock JT. Myoendothelial junctions in human brain arterioles. Stroke. 1991;22(12):1592-7. PubMed PMID: 1962335.

43. Chen B, Friedman B, Cheng Q, Tsai P, Schim E, Kleinfeld D, et al. Severe blood-brain barrier disruption and surrounding tissue injury. Stroke. 2009;40(12):e666-74. Epub 2009/11/05. doi: 10.1161/STROKEAHA.109.551341. PubMed PMID: 19893002; PubMed Central PMCID: PMCPMC2819286.
44. Ramirez SH, Andrews AM, Paul D, Pachter JS. Extracellular vesicles: mediators and biomarkers of pathology along CNS barriers. Fluids Barriers CNS. 2018;15(1):19. Epub 2018/07/01. doi: 10.1186/s12987-018-0104-7. PubMed PMID: 29960602; PubMed Central PMCID: PMCPMC6026502.
45. Dumler JS, Walker DH. Rocky Mountain spotted fever--changing ecology and persisting virulence. N Engl J Med. 2005;353(6):551-3. doi: 10.1056/NEJMp058138. PubMed PMID: 16093463.
46. Chapman AS, Murphy SM, Demma LJ, Holman RC, Curns AT, McQuiston JH, et al. Rocky mountain spotted fever in the United States, 1997-2002. Ann N Y Acad Sci. 2006;1078:154-5. doi: 10.1196/annals.1374.026. PubMed PMID: 17114698.
47. Walker DH, Paddock CD, Dumler JS. Emerging and re-emerging tick-transmitted rickettsial and ehrlichial infections. Med Clin North Am. 2008;92(6):1345-61, x. doi: 10.1016/j.mcna.2008.06.002. PubMed PMID: 19061755.
48. Drexler NA, Dahlgren FS, Heitman KN, Massung RF, Paddock CD, Behravesh CB. National Surveillance of Spotted Fever Group Rickettsioses in the United States, 2008-2012. Am J Trop Med Hyg. 2016;94(1):26-34. Epub 2015/08/31. doi: 10.4269/ajtmh.15-0472. PubMed PMID: 26324732; PubMed Central PMCID: PMCPMC4710440.
49. Saito TB, Bechelli J, Smalley C, Karim S, Walker DH. Vector Tick Transmission Model of Spotted Fever Rickettsiosis. Am J Pathol. 2019;189(1):115-23. Epub 2018/10/11. doi: 10.1016/j.ajpath.2018.09.005. PubMed PMID: 30315767.
50. Chan YG, Riley SP, Martinez JJ. Adherence to and invasion of host cells by spotted Fever group rickettsia species. Front Microbiol. 2010;1:139. doi: 10.3389/fmicb.2010.00139. PubMed PMID: 21687751; PubMed Central PMCID: PMCPMC3109342.
51. Feng HM, Wen J, Walker DH. Rickettsia australis infection: a murine model of a highly invasive vasculopathic rickettsiosis. Am J Pathol. 1993;142(5):1471-82. PubMed PMID: 8494048; PubMed Central PMCID: PMCPMC1886902.
52. Walker DH, Ismail N. Emerging and re-emerging rickettsioses: endothelial cell infection and early disease events. Nat Rev Microbiol. 2008;6(5):375-86. doi: 10.1038/nrmicro1866. PubMed PMID: 18414502.
53. Choe JE, Welch MD. Actin-based motility of bacterial pathogens: mechanistic diversity and its impact on virulence. Pathog Dis. 2016. Epub 2016/09/20. doi: 10.1093/femspd/ftw099. PubMed PMID: 27655913; PubMed Central PMCID: PMCPMC5968334.
54. Felsheim RF, Kurtti TJ, Munderloh UG. Genome sequence of the endosymbiont Rickettsia peacockii and comparison with virulent Rickettsia rickettsii: identification of virulence factors. PLoS One. 2009;4(12):e8361. Epub 2009/12/21. doi: 10.1371/journal.pone.0008361. PubMed PMID: 20027221; PubMed Central PMCID: PMCPMC2791219.
55. Gillespie JJ, Kaur SJ, Rahman MS, Rennoll-Bankert K, Sears KT, Beier-Sexton M, et al. Secretome of obligate intracellular Rickettsia. FEMS Microbiol Rev. 2015;39(1):47-80. Epub 2014/12/04. doi: 10.1111/1574-6976.12084. PubMed PMID: 25168200; PubMed Central PMCID: PMCPMC4344940.
56. Spengler JR, Prescott J, Feldmann H, Spiropoulou CF. Human immune system mouse models of Ebola virus infection. Curr Opin Virol. 2017;25:90-6. Epub 2017/08/12. doi: 10.1016/j.coviro.2017.07.028. PubMed PMID: 28810165; PubMed Central PMCID: PMCPMC5610641.
57. Saphire EO, Aman MJ. Feverish Quest for Ebola Immunotherapy: Straight or Cocktail? Trends Microbiol. 2016;24(9):684-6. Epub 2016/06/20. doi: 10.1016/j.tim.2016.05.008. PubMed PMID: 27338027.

58. Cooper TK, Huzella L, Johnson JC, Rojas O, Yellayi S, Sun MG, et al. Histology, immunohistochemistry, and in situ hybridization reveal overlooked Ebola virus target tissues in the Ebola virus disease guinea pig model. Sci Rep. 2018;8(1):1250. Epub 2018/01/19. doi: 10.1038/s41598-018-19638-x. PubMed PMID: 29352230; PubMed Central PMCID: PMCPMC5775334.
59. Olejnik J, Ryabchikova E, Corley RB, Mühlberger E. Intracellular events and cell fate in filovirus infection. Viruses. 2011;3(8):1501-31. doi: 10.3390/v3081501. PubMed PMID: 21927676; PubMed Central PMCID: PMCPMC3172725.
60. Deflubé LR, Cressey TN, Hume AJ, Olejnik J, Haddock E, Feldmann F, et al. Ebolavirus polymerase uses an unconventional genome replication mechanism. Proc Natl Acad Sci U S A. 2019;116(17):8535-43. Epub 2019/04/08. doi: 10.1073/pnas.1815745116. PubMed PMID: 30962389; PubMed Central PMCID: PMCPMC6486738.
61. Hume A, Mühlberger E. Marburg Virus Viral Protein 35 Inhibits Protein Kinase R Activation in a Cell Type-Specific Manner. J Infect Dis. 2018;218(suppl_5):S403-S8. doi: 10.1093/infdis/jiy473. PubMed PMID: 30165526; PubMed Central PMCID: PMCPMC6249588.
62. Johnson B, Li J, Adhikari J, Edwards MR, Zhang H, Schwarz T, et al. Dimerization Controls Marburg Virus VP24-dependent Modulation of Host Antioxidative Stress Responses. J Mol Biol. 2016;428(17):3483-94. Epub 2016/08/04. doi: 10.1016/j.jmb.2016.07.020. PubMed PMID: 27497688; PubMed Central PMCID: PMCPMC5010500.
63. Edwards MR, Johnson B, Mire CE, Xu W, Shabman RS, Speller LN, et al. The Marburg virus VP24 protein interacts with Keap1 to activate the cytoprotective antioxidant response pathway. Cell Rep. 2014;6(6):1017-25. doi: 10.1016/j.celrep.2014.01.043. PubMed PMID: 24630991; PubMed Central PMCID: PMCPMC3985291.
64. Feldmann H, Geisbert TW. Ebola haemorrhagic fever. Lancet. 2011;377(9768):849-62. doi: 10.1016/S0140-6736(10)60667-8. PubMed PMID: 21084112; PubMed Central PMCID: PMCPMC3406178.
65. Vine V, Scott DP, Feldmann H. Ebolavirus: An Overview of Molecular and Clinical Pathogenesis. Methods Mol Biol. 2017;1628:39-50. doi: 10.1007/978-1-4939-7116-9_3. PubMed PMID: 28573609.
66. Wahl-Jensen VM, Afanasieva TA, Seebach J, Ströher U, Feldmann H, Schnittler HJ. Effects of Ebola virus glycoproteins on endothelial cell activation and barrier function. J Virol. 2005;79(16):10442-50. doi: 10.1128/JVI.79.16.10442-10450.2005. PubMed PMID: 16051836; PubMed Central PMCID: PMCPMC1182673.
67. Wolf T, Kann G, Becker S, Stephan C, Brodt HR, de Leuw P, et al. Severe Ebola virus disease with vascular leakage and multiorgan failure: treatment of a patient in intensive care. Lancet. 2015;385(9976):1428-35. Epub 2014/12/19. doi: 10.1016/S0140-6736(14)62384-9. PubMed PMID: 25534190.
68. Lubaki NM, Ilinykh P, Pietzsch C, Tigabu B, Freiberg AN, Koup RA, et al. The lack of maturation of Ebola virus-infected dendritic cells results from the cooperative effect of at least two viral domains. J Virol. 2013;87(13):7471-85. Epub 2013/04/24. doi: 10.1128/JVI.03316-12. PubMed PMID: 23616668; PubMed Central PMCID: PMCPMC3700277.
69. Martines RB, Ng DL, Greer PW, Rollin PE, Zaki SR. Tissue and cellular tropism, pathology and pathogenesis of Ebola and Marburg viruses. J Pathol. 2015;235(2):153-74. doi: 10.1002/path.4456. PubMed PMID: 25297522.
70. Hayes MJ, Shao D, Bailly M, Moss SE. Regulation of actin dynamics by annexin 2. EMBO J. 2006;25(9):1816-26. doi: 10.1038/sj.emboj.7601078. PubMed PMID: 16601677; PubMed Central PMCID: PMCPMC1456940.
71. Liu Y, Myrvang HK, Dekker LV. Annexin A2 complexes with S100 proteins: structure, function and pharmacological manipulation. Br J Pharmacol. 2014. doi: 10.1111/bph.12978. PubMed PMID: 25303710.

72. Bharadwaj A, Bydoun M, Holloway R, Waisman D. Annexin A2 heterotetramer: structure and function. Int J Mol Sci. 2013;14(3):6259-305. Epub 2013/03/23. doi: 10.3390/ijms14036259. PubMed PMID: 23519104; PubMed Central PMCID: PMCPMC3634455.
73. Grieve AG, Moss SE, Hayes MJ. Annexin A2 at the interface of actin and membrane dynamics: a focus on its roles in endocytosis and cell polarization. Int J Cell Biol. 2012;2012:852430. Epub 2012/04/17. doi: 10.1155/2012/852430. PubMed PMID: 22505935; PubMed Central PMCID: PMCPMC3296266.
74. Rescher U, Ludwig C, Konietzko V, Kharitonenkov A, Gerke V. Tyrosine phosphorylation of annexin A2 regulates Rho-mediated actin rearrangement and cell adhesion. J Cell Sci. 2008;121(Pt 13):2177-85. Epub 2008/06/21. doi: 10.1242/jcs.028415. PubMed PMID: 18565825.
75. Garrido-Gómez T, Dominguez F, Quiñonero A, Estella C, Vilella F, Pellicer A, et al. Annexin A2 is critical for embryo adhesiveness to the human endometrium by RhoA activation through F-actin regulation. FASEB J. 2012;26(9):3715-27. doi: 10.1096/fj.12-204008. PubMed PMID: 22645245.
76. Jung Y, Wang J, Song J, Shiozawa Y, Havens A, Wang Z, et al. Annexin II expressed by osteoblasts and endothelial cells regulates stem cell adhesion, homing, and engraftment following transplantation. Blood. 2007;110(1):82-90. doi: 10.1182/blood-2006-05-021352. PubMed PMID: 17360942; PubMed Central PMCID: PMCPMC1896130.
77. Luo M, Hajjar KA. Annexin A2 system in human biology: cell surface and beyond. Semin Thromb Hemost. 2013;39(4):338-46. doi: 10.1055/s-0033-1334143. PubMed PMID: 23483454; PubMed Central PMCID: PMCPMC3869233.
78. Hajjar KA. The Biology of Annexin A2: From Vascular Fibrinolysis to Innate Immunity. Trans Am Clin Climatol Assoc. 2015;126:144-55. PubMed PMID: 26330668; PubMed Central PMCID: PMCPMC4530673.
79. He X, Zhang W, Chang Q, Su Z, Gong D, Zhou Y, et al. A new role for host annexin A2 in establishing bacterial adhesion to vascular endothelial cells. Laboratory Investigation. 2019;in press.
80. Gong B, Shelite T, Mei FC, Ha T, Hu Y, Xu G, et al. Exchange protein directly activated by cAMP plays a critical role in bacterial invasion during fatal rickettsioses. Proc Natl Acad Sci U S A. 2013;110(48):19615-20. doi: 10.1073/pnas.1314400110. PubMed PMID: 24218580; PubMed Central PMCID: PMCPMC3845138.
81. Lu H, Sun TX, Bouley R, Blackburn K, McLaughlin M, Brown D. Inhibition of endocytosis causes phosphorylation (S256)-independent plasma membrane accumulation of AQP2. Am J Physiol Renal Physiol. 2004;286(2):F233-43. Epub 2003/10/02. doi: 10.1152/ajprenal.00179.2003. PubMed PMID: 14519593.
82. Lokman NA, Ween MP, Oehler MK, Ricciardelli C. The role of annexin A2 in tumorigenesis and cancer progression. Cancer Microenviron. 2011;4(2):199-208. Epub 2011/09/13. doi: 10.1007/s12307-011-0064-9. PubMed PMID: 21909879; PubMed Central PMCID: PMCPMC3170418.
83. Wang S, Sun H, Tanowitz M, Liang XH, Crooke ST. Annexin A2 facilitates endocytic trafficking of antisense oligonucleotides. Nucleic Acids Res. 2016;44(15):7314-30. Epub 2016/07/06. doi: 10.1093/nar/gkw595. PubMed PMID: 27378781; PubMed Central PMCID: PMCPMC5009748.
84. Zhang S, Yu M, Guo Q, Li R, Li G, Tan S, et al. Annexin A2 binds to endosomes and negatively regulates TLR4-triggered inflammatory responses via the TRAM-TRIF pathway. Sci Rep. 2015;5:15859. Epub 2015/11/04. doi: 10.1038/srep15859. PubMed PMID: 26527544; PubMed Central PMCID: PMCPMC4630631.
85. Law AL, Ling Q, Hajjar KA, Futter CE, Greenwood J, Adamson P, et al. Annexin A2 regulates phagocytosis of photoreceptor outer segments in the mouse retina. Mol Biol Cell. 2009;20(17):3896-904. Epub 2009/07/10. doi: 10.1091/mbc.E08-12-1204. PubMed PMID: 19587120; PubMed Central PMCID: PMCPMC2735488.

86. Morozova K, Sridhar S, Zolla V, Clement CC, Scharf B, Verzani Z, et al. Annexin A2 promotes phagophore assembly by enhancing Atg16L(+) vesicle biogenesis and homotypic fusion. Nat Commun. 2015;6:5856. Epub 2015/01/20. doi: 10.1038/ncomms6856. PubMed PMID: 25597631; PubMed Central PMCID: PMCPMC4299943.
87. Rentero C, Blanco-Munoz P, Meneses-Salas E, Grewal T, Enrich C. Annexins-Coordinators of Cholesterol Homeostasis in Endocytic Pathways. Int J Mol Sci. 2018;19(5). Epub 2018/05/15. doi: 10.3390/ijms19051444. PubMed PMID: 29757220; PubMed Central PMCID: PMCPMC5983649.
88. Maiers JL, Peng X, Fanning AS, DeMali KA. ZO-1 recruitment to alpha-catenin--a novel mechanism for coupling the assembly of tight junctions to adherens junctions. J Cell Sci. 2013;126(Pt 17):3904-15. Epub 2013/07/03. doi: 10.1242/jcs.126565. PubMed PMID: 23813953; PubMed Central PMCID: PMCPMC3757330.
89. Bray M, Davis K, Geisbert T, Schmaljohn C, Huggins J. A mouse model for evaluation of prophylaxis and therapy of Ebola hemorrhagic fever. J Infect Dis. 1998;178(3):651-61. PubMed PMID: 9728532.
90. Ling Q, Jacovina AT, Deora A, Febbraio M, Simantov R, Silverstein RL, et al. Annexin II regulates fibrin homeostasis and neoangiogenesis in vivo. J Clin Invest. 2004;113(1):38-48. doi: 10.1172/JCI19684. PubMed PMID: 14702107; PubMed Central PMCID: PMCPMC300771.
91. Libby P. Once more unto the breach: endothelial permeability and atherogenesis. Eur Heart J. 2019;40(11):938-40. Epub 2019/02/26. doi: 10.1093/eurheartj/ehz081. PubMed PMID: 30805590.
92. He X, Drelich A, Yu S, Chang Q, Gong D, Zhou Y, et al. Exchange protein directly activated by cAMP plays a critical role in regulation of vascular fibrinolysis. Life Sci. 2019;221:1-12. Epub 2019/02/07. doi: 10.1016/j.lfs.2019.02.014. PubMed PMID: 30738042.
93. Campbell HK, Maiers JL, DeMali KA. Interplay between tight junctions & adherens junctions. Exp Cell Res. 2017;358(1):39-44. Epub 2017/03/31. doi: 10.1016/j.yexcr.2017.03.061. PubMed PMID: 28372972; PubMed Central PMCID: PMCPMC5544570.
94. Antonov A, Snead C, Gorshkov B, Antonova GN, Verin AD, Catravas JD. Heat shock protein 90 inhibitors protect and restore pulmonary endothelial barrier function. Am J Respir Cell Mol Biol. 2008;39(5):551-9. Epub 2008/05/14. doi: 10.1165/rcmb.2007-0324OC. PubMed PMID: 18474672; PubMed Central PMCID: PMCPMC2574526.
95. Chatterjee A, Snead C, Yetik-Anacak G, Antonova G, Zeng J, Catravas JD. Heat shock protein 90 inhibitors attenuate LPS-induced endothelial hyperpermeability. Am J Physiol Lung Cell Mol Physiol. 2008;294(4):L755-63. Epub 2008/02/05. doi: 10.1152/ajplung.00350.2007. PubMed PMID: 18245267.
96. Joshi AD, Dimitropoulou C, Thangjam G, Snead C, Feldman S, Barabutis N, et al. Heat shock protein 90 inhibitors prevent LPS-induced endothelial barrier dysfunction by disrupting RhoA signaling. Am J Respir Cell Mol Biol. 2014;50(1):170-9. Epub 2013/08/27. doi: 10.1165/rcmb.2012-0496OC. PubMed PMID: 23972231; PubMed Central PMCID: PMCPMC3930930.
97. Stenos J, Walker DH. The rickettsial outer-membrane protein A and B genes of Rickettsia australis, the most divergent rickettsia of the spotted fever group. Int J Syst Evol Microbiol. 2000;50 Pt 5:1775-9. Epub 2000/10/18. doi: 10.1099/00207713-50-5-1775. PubMed PMID: 11034486.
98. Lei H, Romeo G, Kazlauskas A. Heat shock protein 90alpha-dependent translocation of annexin II to the surface of endothelial cells modulates plasmin activity in the diabetic rat aorta. Circ Res. 2004;94(7):902-9. Epub 2004/03/06. doi: 10.1161/01.RES.0000124979.46214.E3. PubMed PMID: 15001530.
99. Tojkander S, Gateva G, Lappalainen P. Actin stress fibers--assembly, dynamics and biological roles. J Cell Sci. 2012;125(Pt 8):1855-64. Epub 2012/05/01. doi: 10.1242/jcs.098087. PubMed PMID: 22544950.

100. Colombelli J, Besser A, Kress H, Reynaud EG, Girard P, Caussinus E, et al. Mechanosensing in actin stress fibers revealed by a close correlation between force and protein localization. J Cell Sci. 2009;122(Pt 10):1665-79. Epub 2009/04/30. doi: 10.1242/jcs.042986. PubMed PMID: 19401336.
101. Hoelzle MK, Svitkina T. The cytoskeletal mechanisms of cell-cell junction formation in endothelial cells. Mol Biol Cell. 2012;23(2):310-23. Epub 2011/11/18. doi: 10.1091/mbc.E11-08-0719. PubMed PMID: 22090347; PubMed Central PMCID: PMCPMC3258175.
102. Tinsley JH, Wu MH, Ma W, Taulman AC, Yuan SY. Activated neutrophils induce hyperpermeability and phosphorylation of adherens junction proteins in coronary venular endothelial cells. J Biol Chem. 1999;274(35):24930-4. Epub 1999/08/24. doi: 10.1074/jbc.274.35.24930. PubMed PMID: 10455168.
103. Sun H, Breslin JW, Zhu J, Yuan SY, Wu MH. Rho and ROCK signaling in VEGF-induced microvascular endothelial hyperpermeability. Microcirculation. 2006;13(3):237-47. Epub 2006/04/22. doi: 10.1080/10739680600556944. PubMed PMID: 16627366.
104. Georgiou M, Marinari E, Burden J, Baum B. Cdc42, Par6, and aPKC regulate Arp2/3-mediated endocytosis to control local adherens junction stability. Curr Biol. 2008;18(21):1631-8. Epub 2008/11/04. doi: 10.1016/j.cub.2008.09.029. PubMed PMID: 18976918.
105. Gerhardt H, Wolburg H, Redies C. N-cadherin mediates pericytic-endothelial interaction during brain angiogenesis in the chicken. Dev Dyn. 2000;218(3):472-9. Epub 2000/07/06. doi: 10.1002/1097-0177(200007)218:3<472::AID-DVDY1008>3.0.CO;2-#. PubMed PMID: 10878612.
106. Fiorini C, Gilleron J, Carette D, Valette A, Tilloy A, Chevalier S, et al. Accelerated internalization of junctional membrane proteins (connexin 43, N-cadherin and ZO-1) within endocytic vacuoles: an early event of DDT carcinogenicity. Biochim Biophys Acta. 2008;1778(1):56-67. Epub 2007/10/24. doi: 10.1016/j.bbamem.2007.08.032. PubMed PMID: 17949680.
107. Eddinger TJ, Schiebout JD, Swartz DR. Adherens junction-associated protein distribution differs in smooth muscle tissue and acutely isolated cells. Am J Physiol Gastrointest Liver Physiol. 2007;292(2):G684-97. Epub 2006/10/21. doi: 10.1152/ajpgi.00277.2006. PubMed PMID: 17053160.
108. Alanko J, Ivaska J. Endosomes: Emerging Platforms for Integrin-Mediated FAK Signalling. Trends Cell Biol. 2016;26(6):391-8. Epub 2016/03/06. doi: 10.1016/j.tcb.2016.02.001. PubMed PMID: 26944773.
109. Qi J, Liu Y, Yang P, Chen T, Liu XZ, Yin Y, et al. Heat shock protein 90 inhibition by 17-Dimethylaminoethylamino-17-demethoxygeldanamycin protects blood-brain barrier integrity in cerebral ischemic stroke. Am J Transl Res. 2015;7(10):1826-37. Epub 2015/12/23. PubMed PMID: 26692927; PubMed Central PMCID: PMCPMC4656760.
110. Poulaki V, Iliaki E, Mitsiades N, Mitsiades CS, Paulus YN, Bula DV, et al. Inhibition of Hsp90 attenuates inflammation in endotoxin-induced uveitis. FASEB J. 2007;21(9):2113-23. Epub 2007/04/03. doi: 10.1096/fj.06-7637com. PubMed PMID: 17400913.
111. Shimp SK, 3rd, Parson CD, Regna NL, Thomas AN, Chafin CB, Reilly CM, et al. HSP90 inhibition by 17-DMAG reduces inflammation in J774 macrophages through suppression of Akt and nuclear factor-kappaB pathways. Inflamm Res. 2012;61(5):521-33. Epub 2012/02/14. doi: 10.1007/s00011-012-0442-x. PubMed PMID: 22327510.
112. Akhter S, Chakraborty S, Moutinho D, Alvarez-Coiradas E, Rosa I, Vinuela J, et al. The human VGF-derived bioactive peptide TLQP-21 binds heat shock 71 kDa protein 8 (HSPA8)on the surface of SH-SY5Y cells. PLoS One. 2017;12(9):e0185176. Epub 2017/09/22. doi: 10.1371/journal.pone.0185176. PubMed PMID: 28934328; PubMed Central PMCID: PMCPMC5608341.
113. Bonam SR, Ruff M, Muller S. HSPA8/HSC70 in Immune Disorders: A Molecular Rheostat that Adjusts Chaperone-Mediated Autophagy Substrates. Cells. 2019;8(8). Epub 2019/08/10. doi: 10.3390/cells8080849. PubMed PMID: 31394830.

114. Kyriakis JM, Avruch J. Mammalian MAPK signal transduction pathways activated by stress and inflammation: a 10-year update. Physiol Rev. 2012;92(2):689-737. Epub 2012/04/27. doi: 10.1152/physrev.00028.2011. PubMed PMID: 22535895.
115. Madureira PA, Hill R, Miller VA, Giacomantonio C, Lee PW, Waisman DM. Annexin A2 is a novel cellular redox regulatory protein involved in tumorigenesis. Oncotarget. 2011;2(12):1075-93. Epub 2011/12/22. doi: 10.18632/oncotarget.375. PubMed PMID: 22185818; PubMed Central PMCID: PMCPMC3282068.
116. Gong B, Lee YS, Lee I, Shelite TR, Kunkeaw N, Xu G, et al. Compartmentalized, functional role of angiogenin during spotted fever group rickettsia-induced endothelial barrier dysfunction: evidence of possible mediation by host tRNA-derived small noncoding RNAs. BMC Infect Dis. 2013;13:285. doi: 10.1186/1471-2334-13-285. PubMed PMID: 23800282; PubMed Central PMCID: PMCPMC3699377.
117. Smalley C, Bechelli J, Rockx-Brouwer D, Saito T, Azar SR, Ismail N, et al. Rickettsia australis Activates Inflammasome in Human and Murine Macrophages. PLoS One. 2016;11(6):e0157231. Epub 2016/07/01. doi: 10.1371/journal.pone.0157231. PubMed PMID: 27362650; PubMed Central PMCID: PMCPMC4928923.
118. Nesvizhskii AI, Keller A, Kolker E, Aebersold R. A statistical model for identifying proteins by tandem mass spectrometry. Anal Chem. 2003;75(17):4646-58. Epub 2003/11/25. doi: 10.1021/ac0341261. PubMed PMID: 14632076.
119. Maere S, Heymans K, Kuiper M. BiNGO: a Cytoscape plugin to assess overrepresentation of gene ontology categories in biological networks. Bioinformatics. 2005;21(16):3448-9. Epub 2005/06/24. doi: 10.1093/bioinformatics/bti551. PubMed PMID: 15972284.
120. Mostafavi S, Ray D, Warde-Farley D, Grouios C, Morris Q. GeneMANIA: a real-time multiple association network integration algorithm for predicting gene function. Genome Biol. 2008;9 Suppl 1:S4. Epub 2008/07/22. doi: 10.1186/gb-2008-9-s1-s4. PubMed PMID: 18613948; PubMed Central PMCID: PMCPMC2447538.

Supporting Information Legends

Supplemental Figure 1. (A) Comparing the survival of ANXA2-KO (n=15) and WT (n=14) mice challenged by R.australis up to 10 days. No significant difference was found based on Log-rank test. (B) Gross view of the brain surface (R. australis infected WT(top panel) & R.australis infected KO (bottom panel)). Yellow arrows indicate R. australis infected mice brains exhibt a large difference in color.

Supplemental Figure 2. Comparing the survival of ANXA2-KO and WT mice challenged by Ebola virus up to 12 days. No significant difference was found based on Log-rank test, n=5 for both groups, P=0.08.

Figure legends

Figure 1. Representative H&E staining of the brains from *R.australlis*-infected *ANXA2*-KO and WT mice. Yellow arrows indicate the presence of focal hemorrhagic lesions. A, mock WT; B&C, mock *AXNA2*-KO; D-F, *R. australis*-infected WT; G-L), *R. australis*-infected *AXNA2*-KO mice. Scale bar: 20 μm.

Figure 2. Representative H&E staining of brain sections from WT (A&B) and *ANXA2*-KO (C&D) 5 days post-*R. australis* infection. Perivascular hemorrhage (yellow arrow) can be observed in infected *ANXA2*-KO group but not infected WT group. TNFα (E) and IFNγ (F) concentrations in serum at 2,4,5 days post-*R. australis* infection. Relative R. australis DNA copies (G) extracted from the brain of WT and *ANXA2*-KO mice quantified by rt-qPCR. No significant difference was found. Error bar stands for standard deviation. Scale bar: 20 μm.

Figure 3. Representative IF staining of SFG rickettsiae (green) in livers, brains and lungs from WT and *ANXA2*-KO mice while nuclei of mouse cells were counter-stained with DAPI (blue). The areas indicated by the arrows are enlarged and distinguish rickettsial (green) staining (boxed inserts). Scale bars, 20 μm.

Figure 4. Functional annotation from Go Term and KEGG for whole-brain lysate.

Figure 5. Functional annotation from Go Term and KEGG for isolated endosomes from the brain.

Figure 6. Functional group from GO Term Cellular Component (A) and DE protein-protein interaction network visualization (B) for whole-brain lysate.

Figure 7. Functional group from GO Term Cellular Component (A) and DE protein-protein interaction network visualization (B) for brain-derived endosome.

Figure 8. (A) Representative IF staining of ZO-1 (left) and occludin (right) in the brains from *R.australis*/mock-infected/ WT and *ANXA2*-KO mice, at day 5 p.i.. Yellow arrows indicate the fragmented structures of ZO-1 and occludin, which were mainly seen in infected *ANXA2*-KO mice. (B) Representative IF staining for occludin in the livers from *R.australis*/mock-infected/ WT and *ANXA2*-KO mice, at day 5 p.i.. (C) Representative IF for VE-cadherin in the brains from *R.australis*/mock-infected/ WT and *ANXA2*-KO mice, at day 5 p.i. Yellow arrows indicate the fragmented structures of VE-cadherin. Nuclei of mouse cells were counterstained with DAPI (blue). Scale bar: 20um.

Figure 9. (A) Representative IF for Ebola virus antigen (Green) in the brains, livers, and lungs from WT or *ANXA2*-KO mice post-Ebola virus challenge. Yellow arrows represent the presence of Ebola virus antigen. (B-E) H&E staining of the brain from WT(B) and *ANXA2*-KO (C-E) mice infected by Ebola virus. Yellow arrows indicate the presence of perivascular hemorrhage. (F) Representative IF for ZO-1 (left) and Occludin (right) in the brains from WT or *ANXA2*-KO mice post-Ebola virus challenge. Yellow arrows indicate the position of ZO-1 or occludin, which represent the tight junction structure. *ANXA2*-KO but not WT Ebola virus-infected mice exhibited the fragmented tight junction structure in the brain. (G) Representative IF for occludin (red) in the livers from WT or *ANXA*2-KO mice day 10 post Ebola virus challenge. Yellow arrows show the structure of the pericellular occludin, which was relatively intact in Ebola virus-infected WT mice but dramatically fragmented in the Ebola virus-infected *ANXA2-KO* mice. Nuclei of mouse cells were counterstained with DAPI (blue). Scale bar: 50 μm (A-E), 20 μm (F and G).

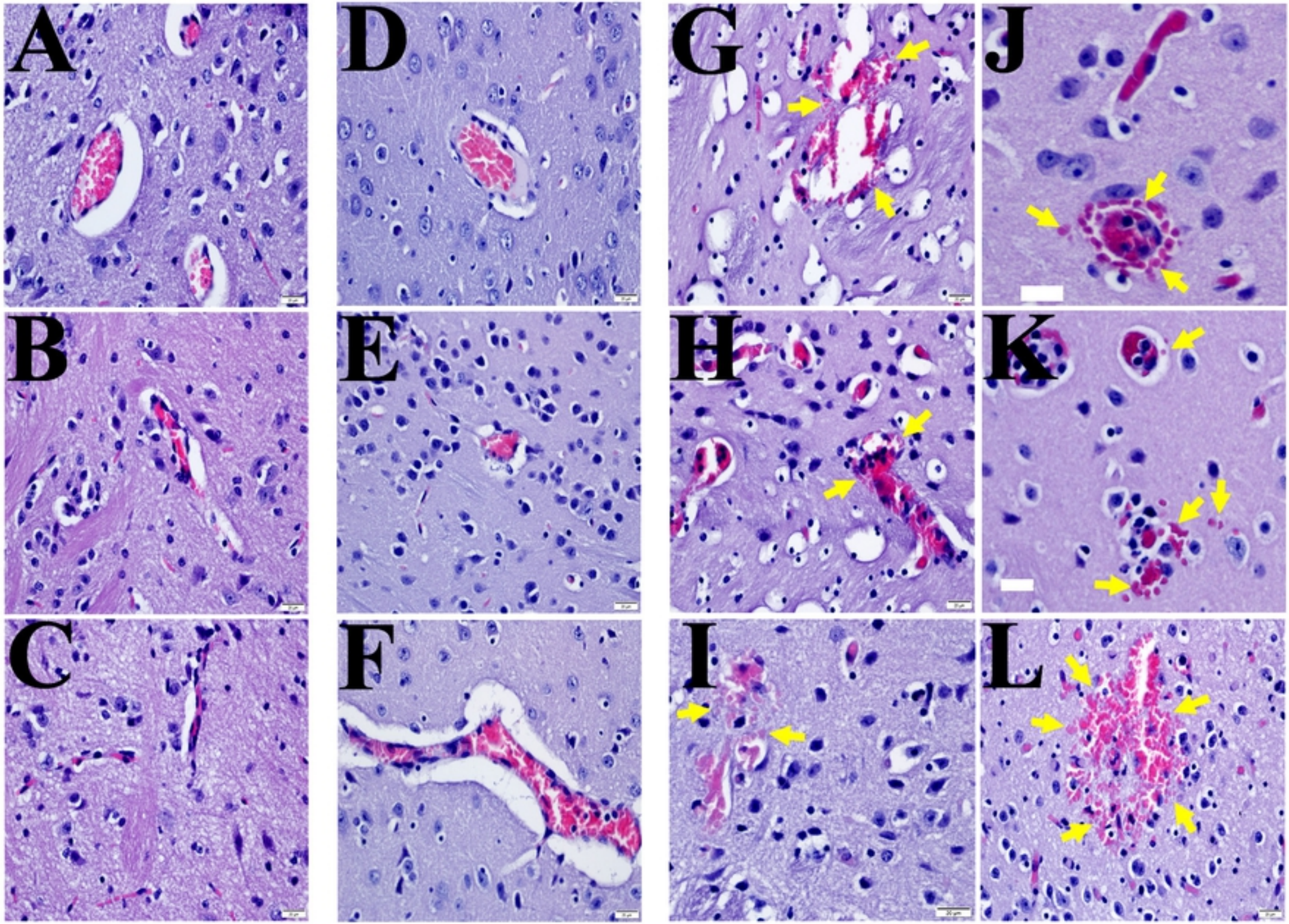

Fig 1

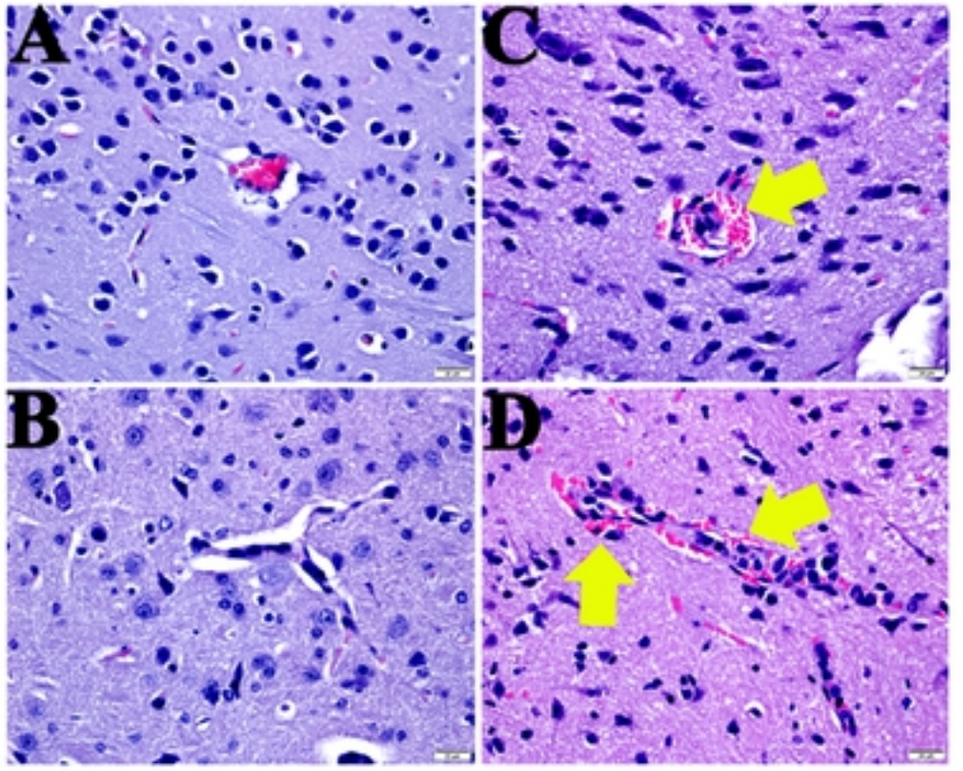
A
C
B
D

E

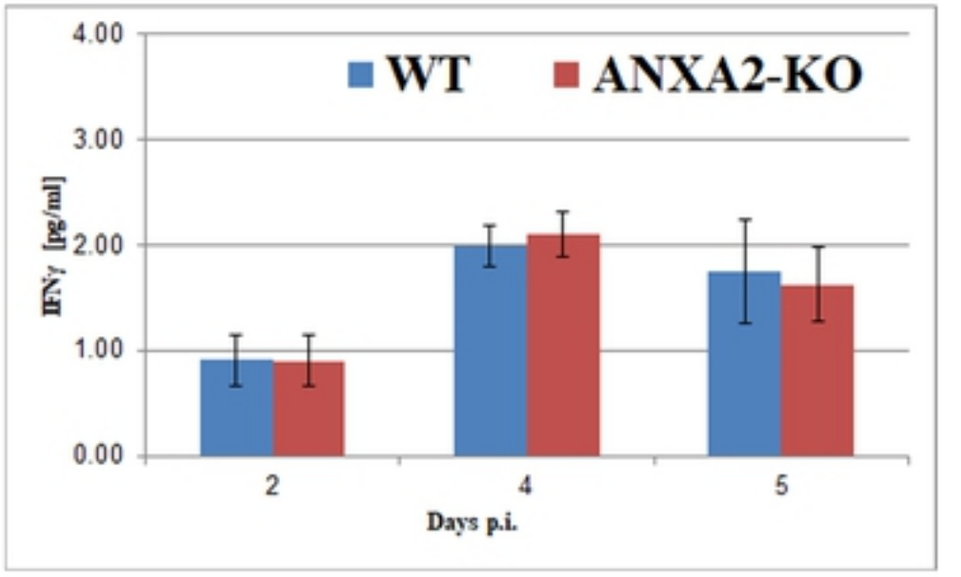
4.00
3.00
2.00
1.00
0.00
IFNγ [pg/ml]
WT
ANXA2-KO
2
4
5
Days p.i.

F

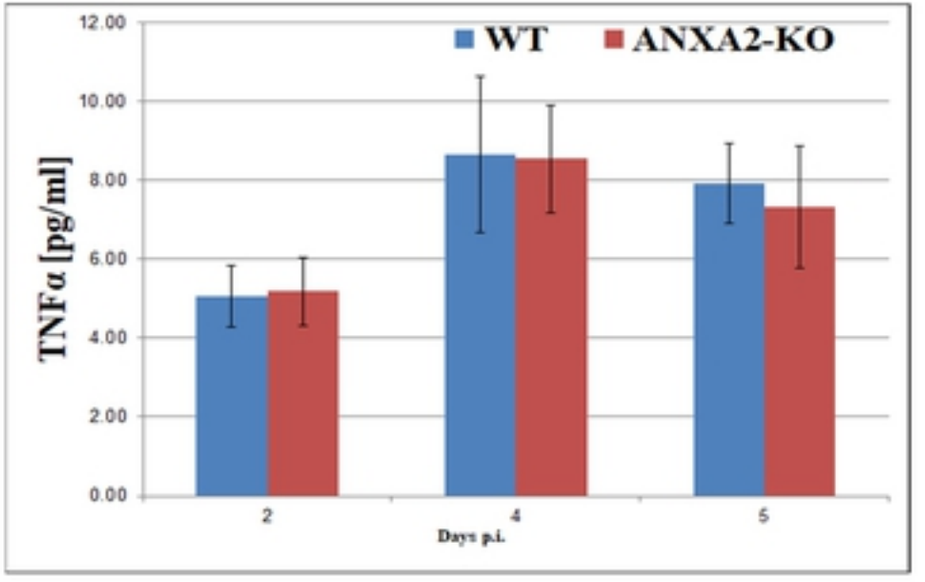
12.00
10.00
8.00
6.00
4.00
2.00
0.00
TNFα [pg/ml]
WT
ANXA2-KO
2
4
5
Days p.i.

G

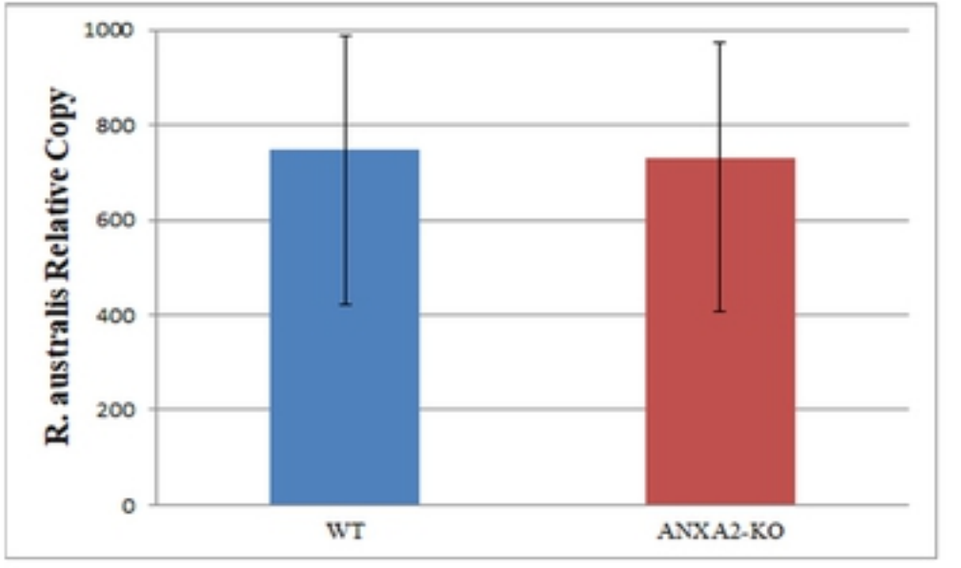
1000
800
600
400
200
0
R. australis Relative Copy
WT
ANXA2-KO

Fig 2

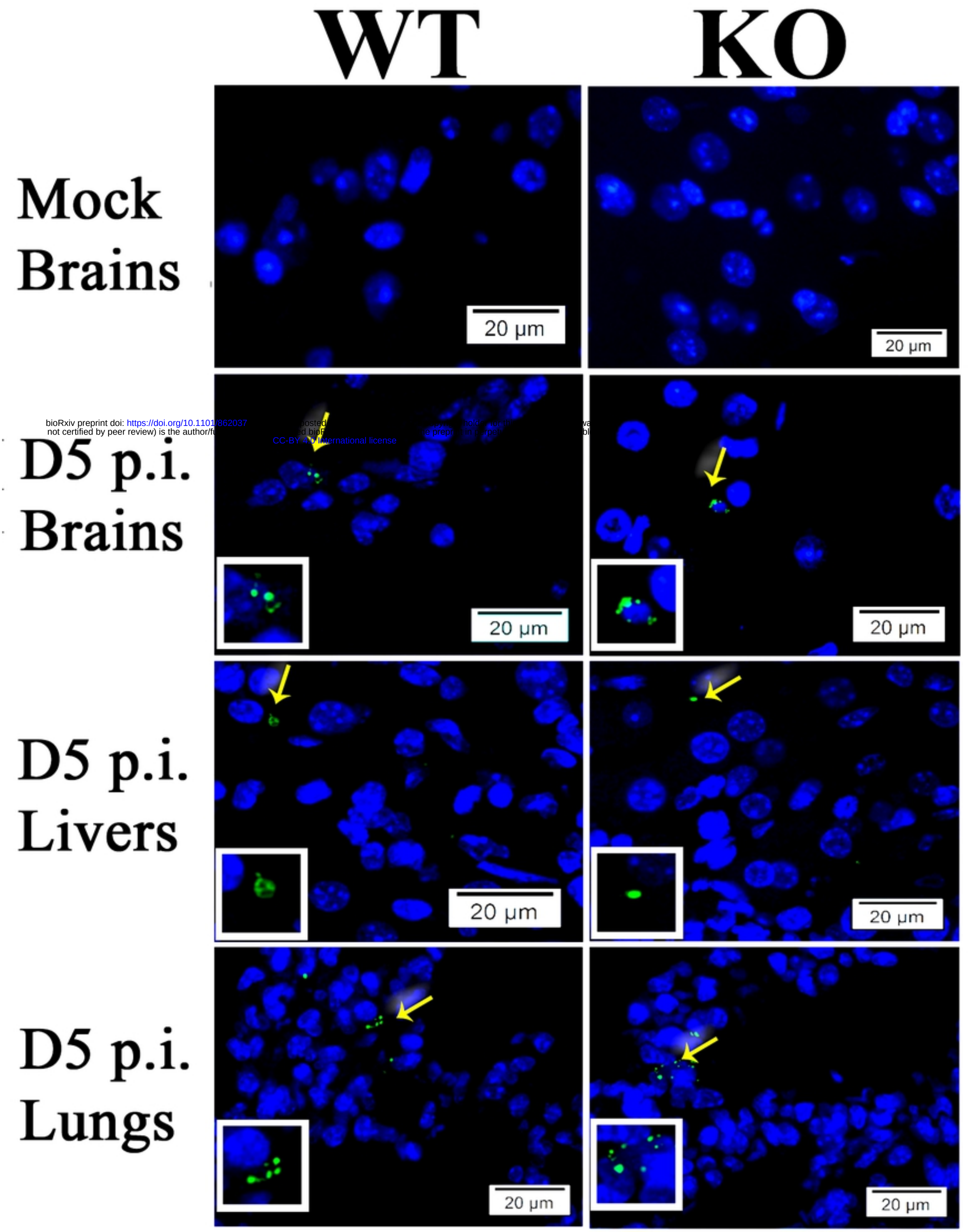

Fig 3

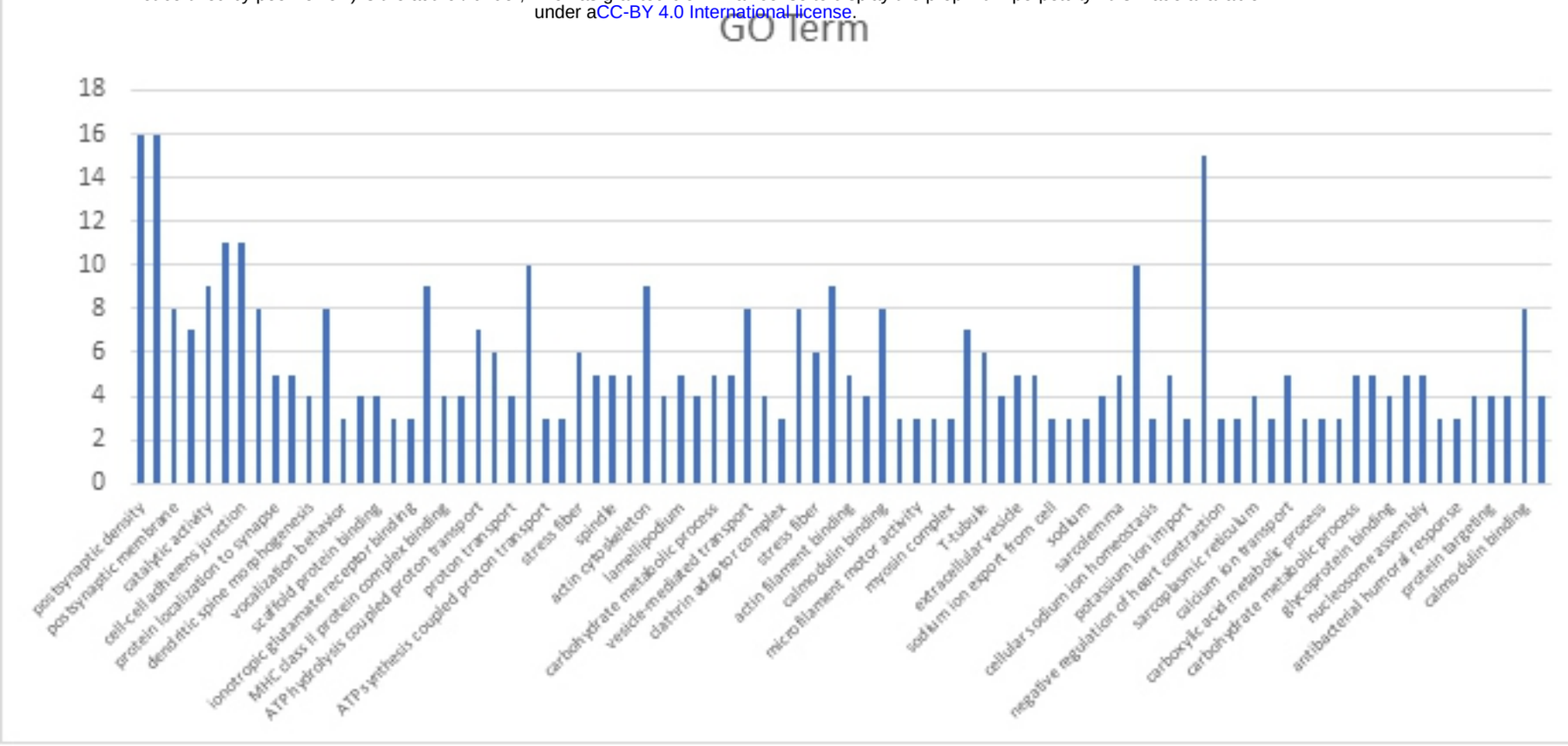

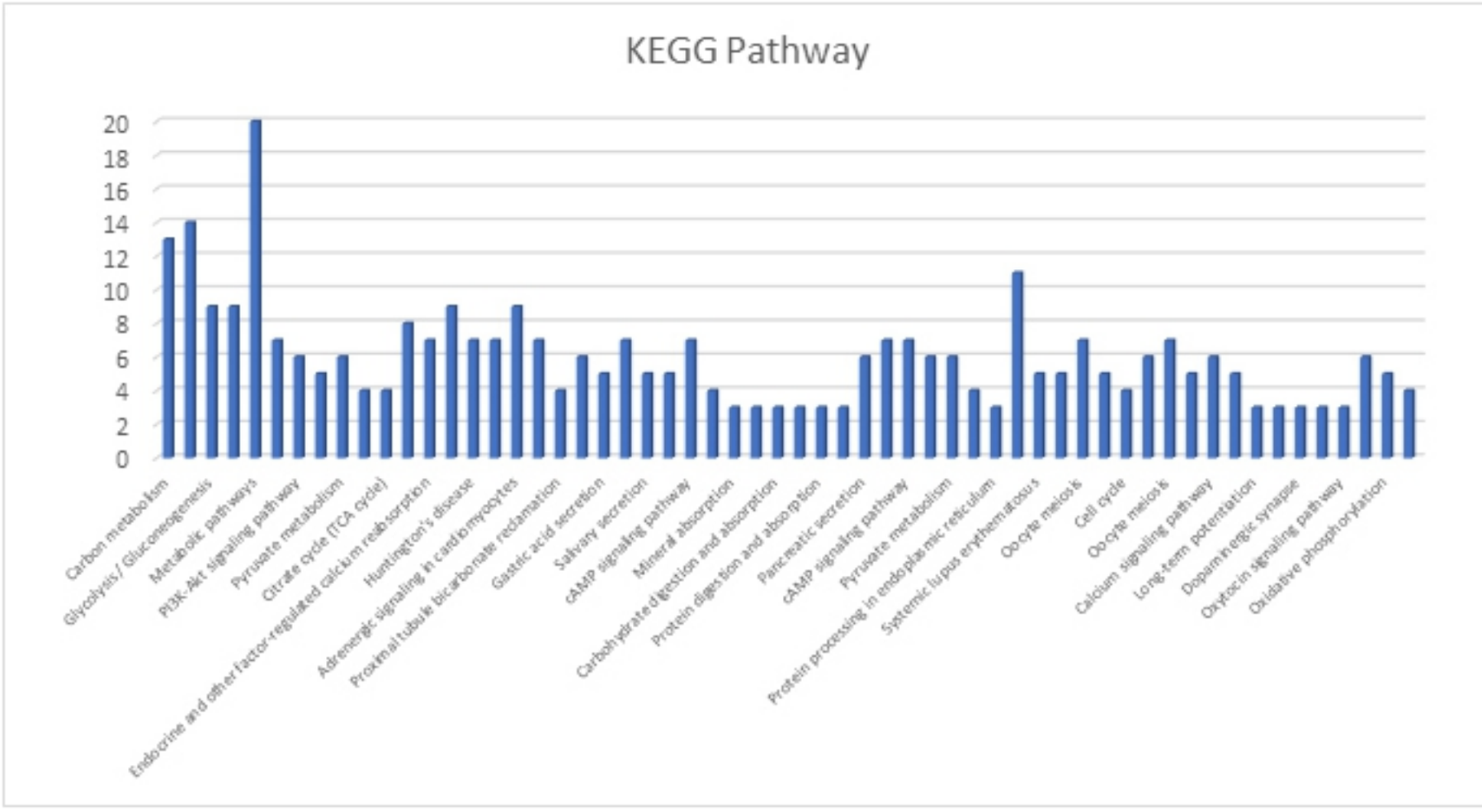

Fig 4

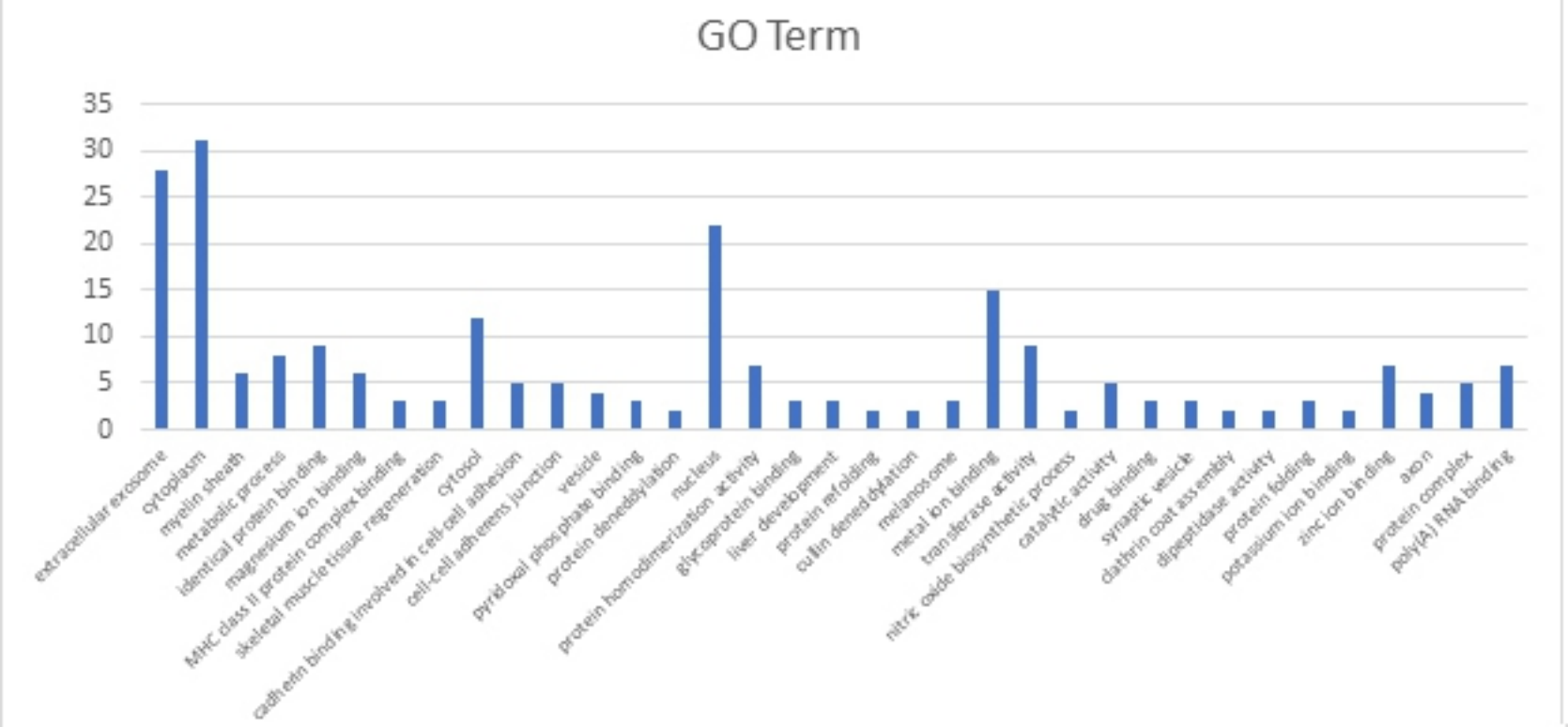
GO Term
35
30
25
20
15
10
5
0
extracellular exosome
cytoplasm
myelin sheath
metabolic process
identical protein binding
magnesium ion binding
MHC class II protein complex binding
skeletal muscle tissue regeneration
cytosol
cadherin binding involved in cell-cell adhesion
cell-cell adherens junction
vesicle
Pyridoxal phosphate binding
protein deneddylation
nucleus
protein homodimerization activity
glycoprotein binding
liver development
protein refolding
cullin deneddylation
melanosome
metal ion binding
transferase activity
nitric oxide biosynthetic process
catalytic activity
drug binding
synaptic vesicle
clathrin coat assembly
dipeptidase activity
protein folding
potassium ion binding
zinc ion binding
axon
protein complex
poly(A) RNA binding

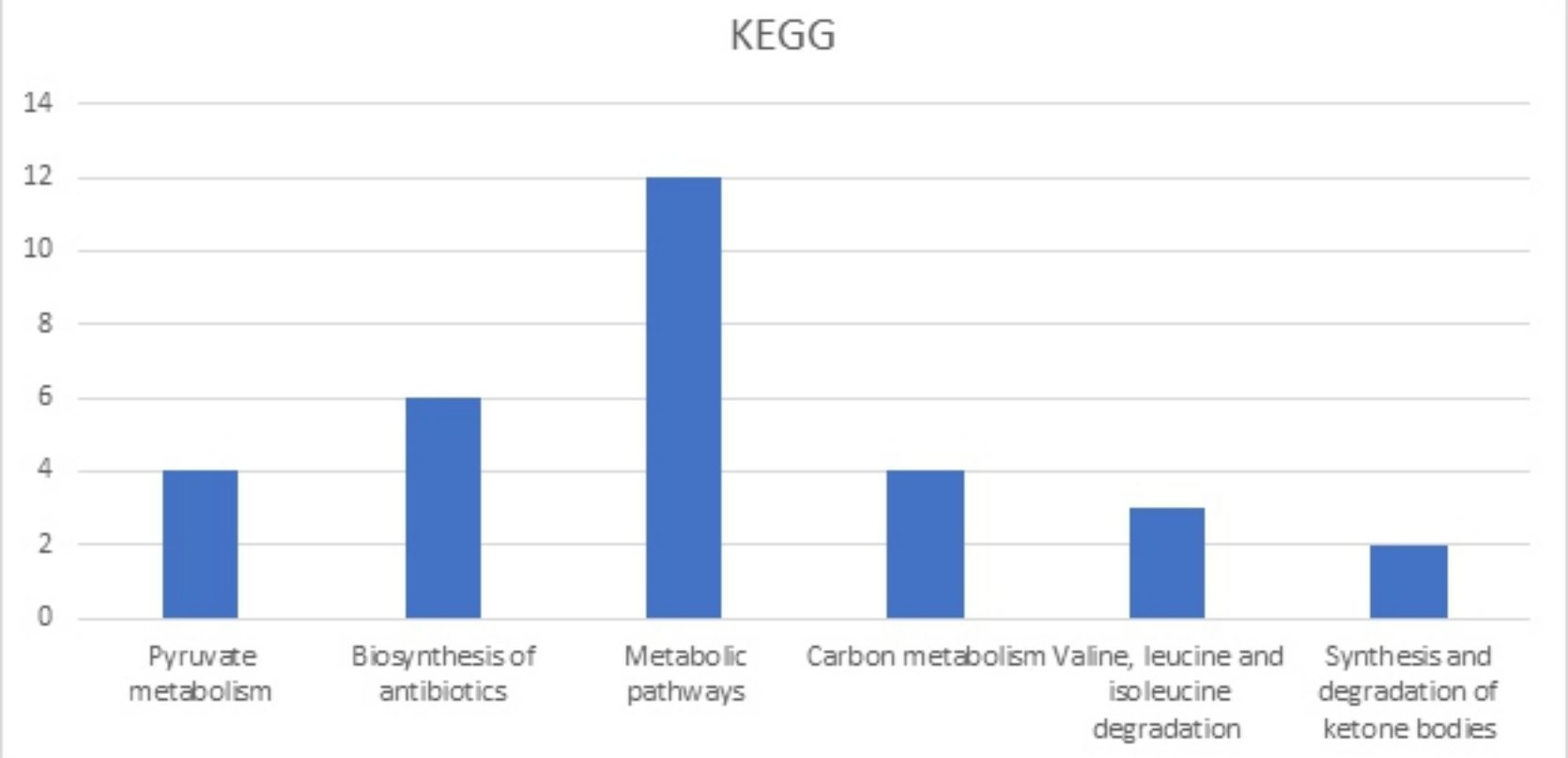
KEGG
14
12
10
8
6
4
2
0
Pyruvate metabolism
Biosynthesis of antibiotics
Metabolic pathways
Carbon metabolism
Valine, leucine and isoleucine degradation
Synthesis and degradation of ketone bodies

Fig 5

A

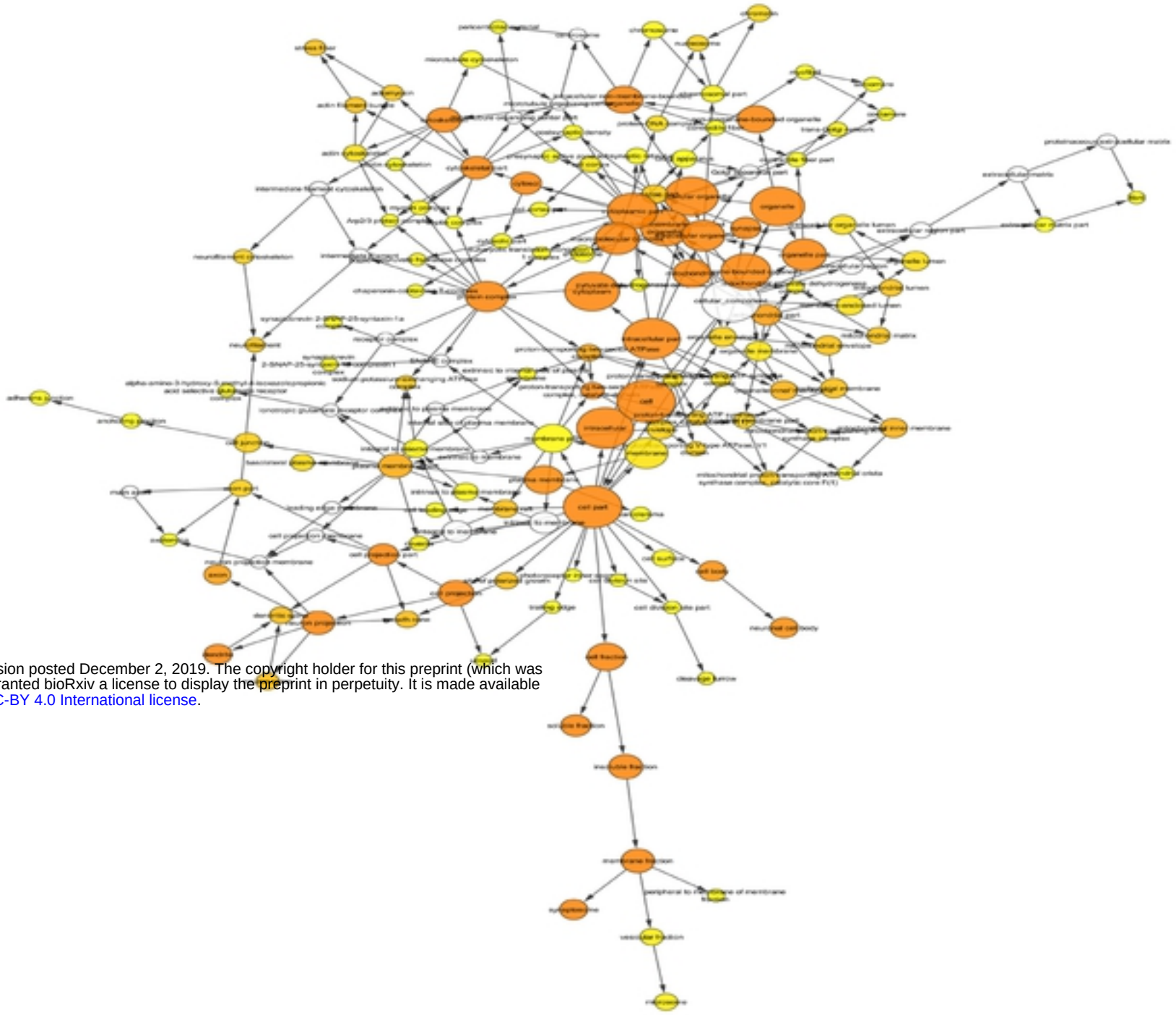

B

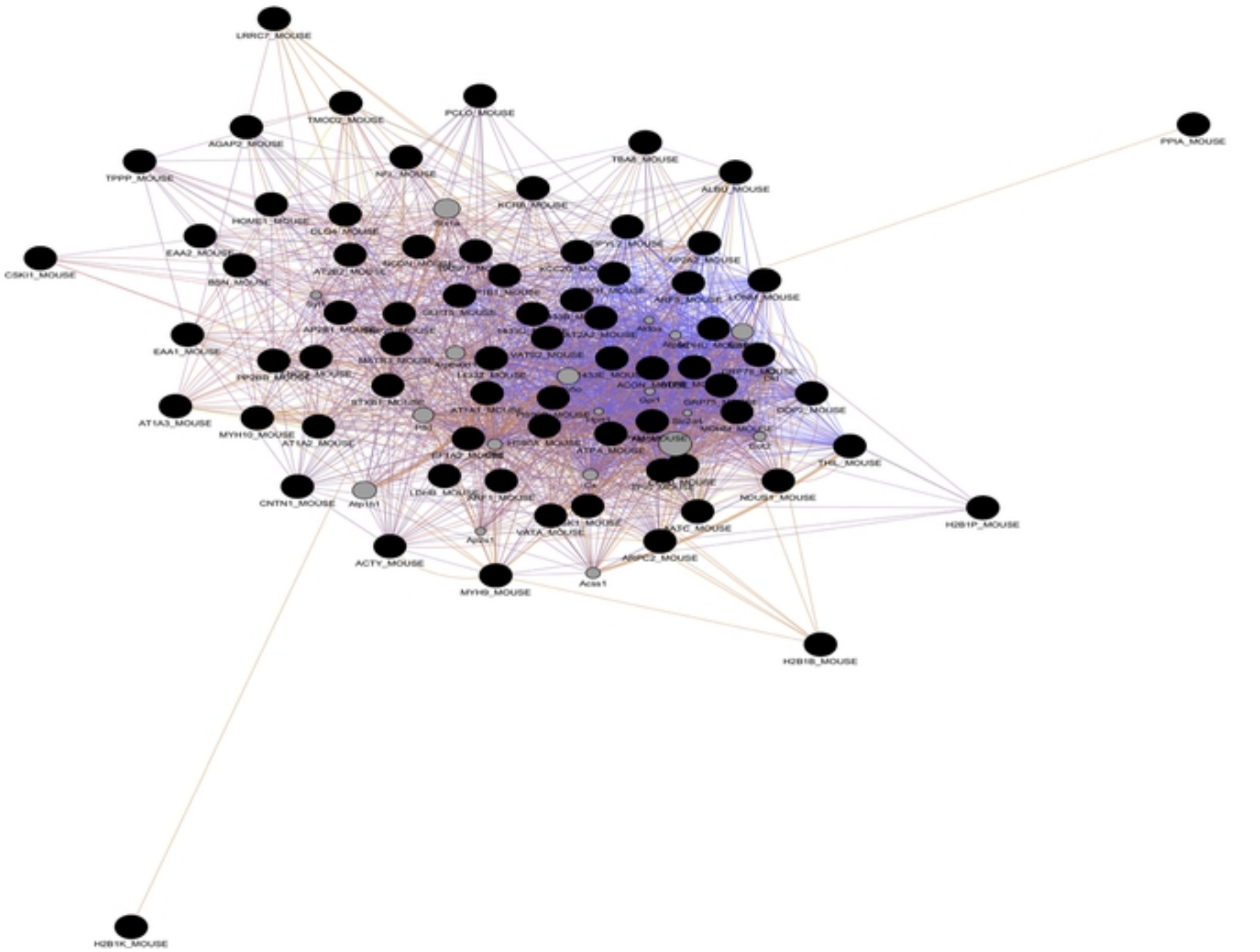

Fig 6

A

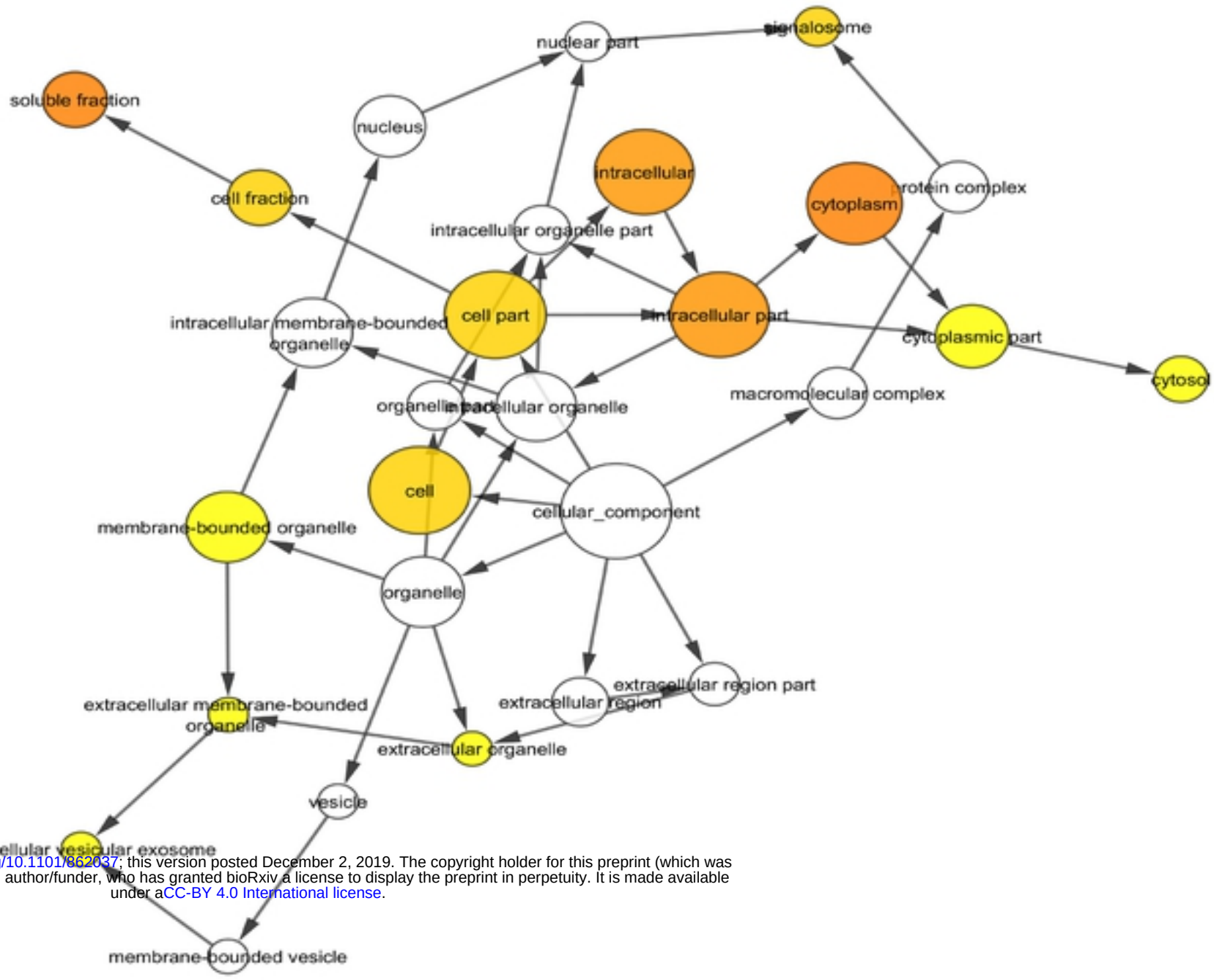

B

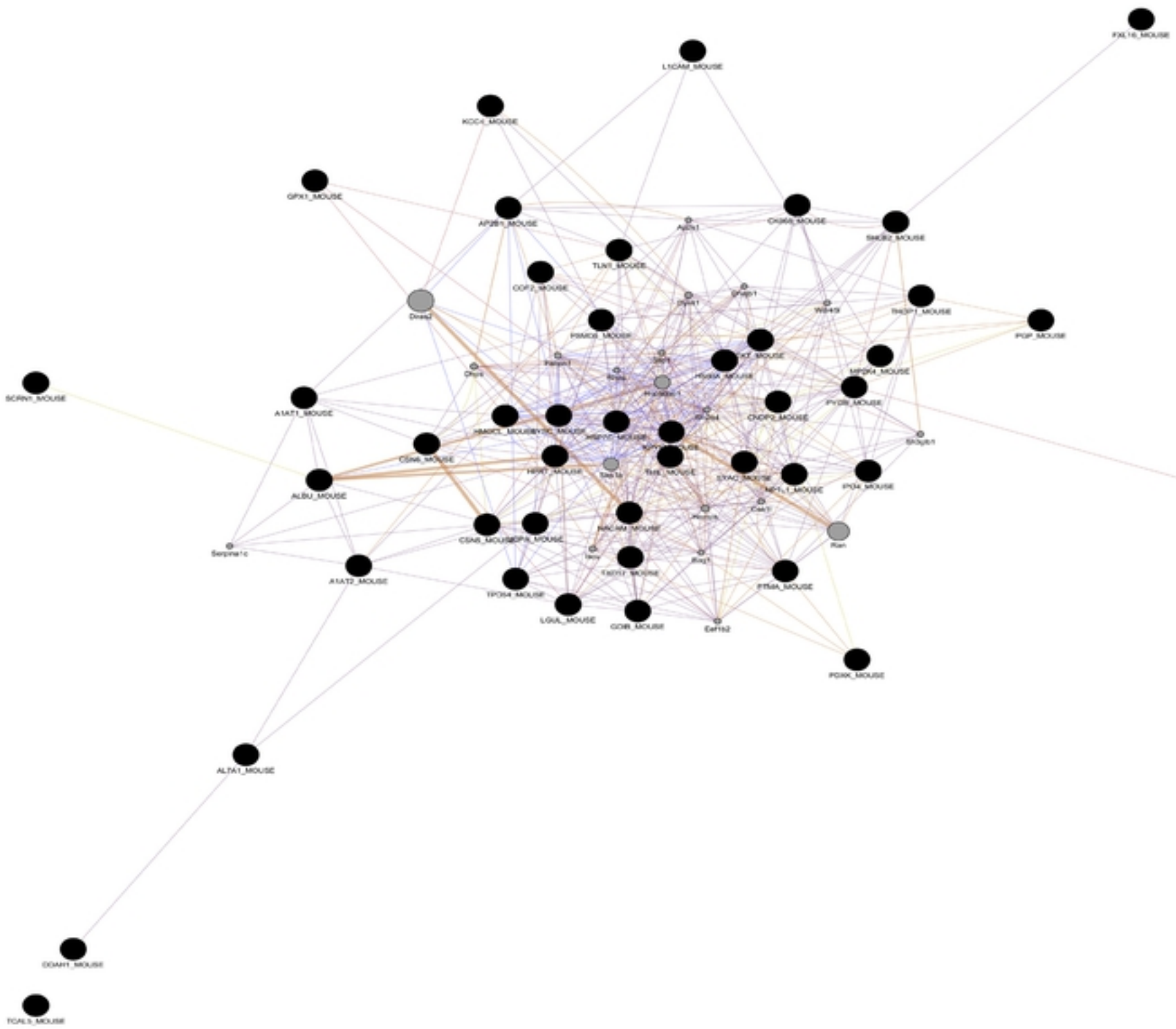

Fig 7

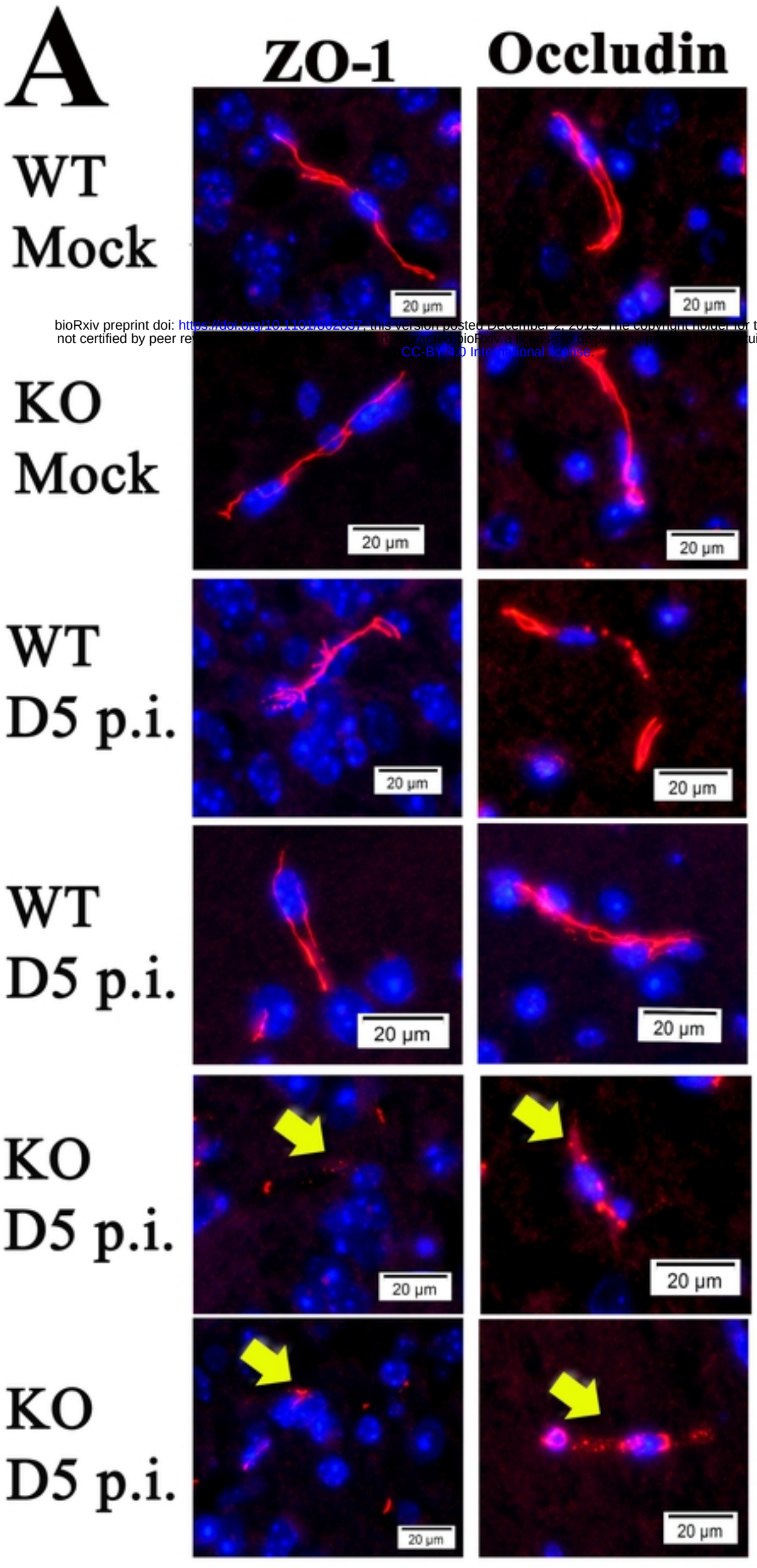

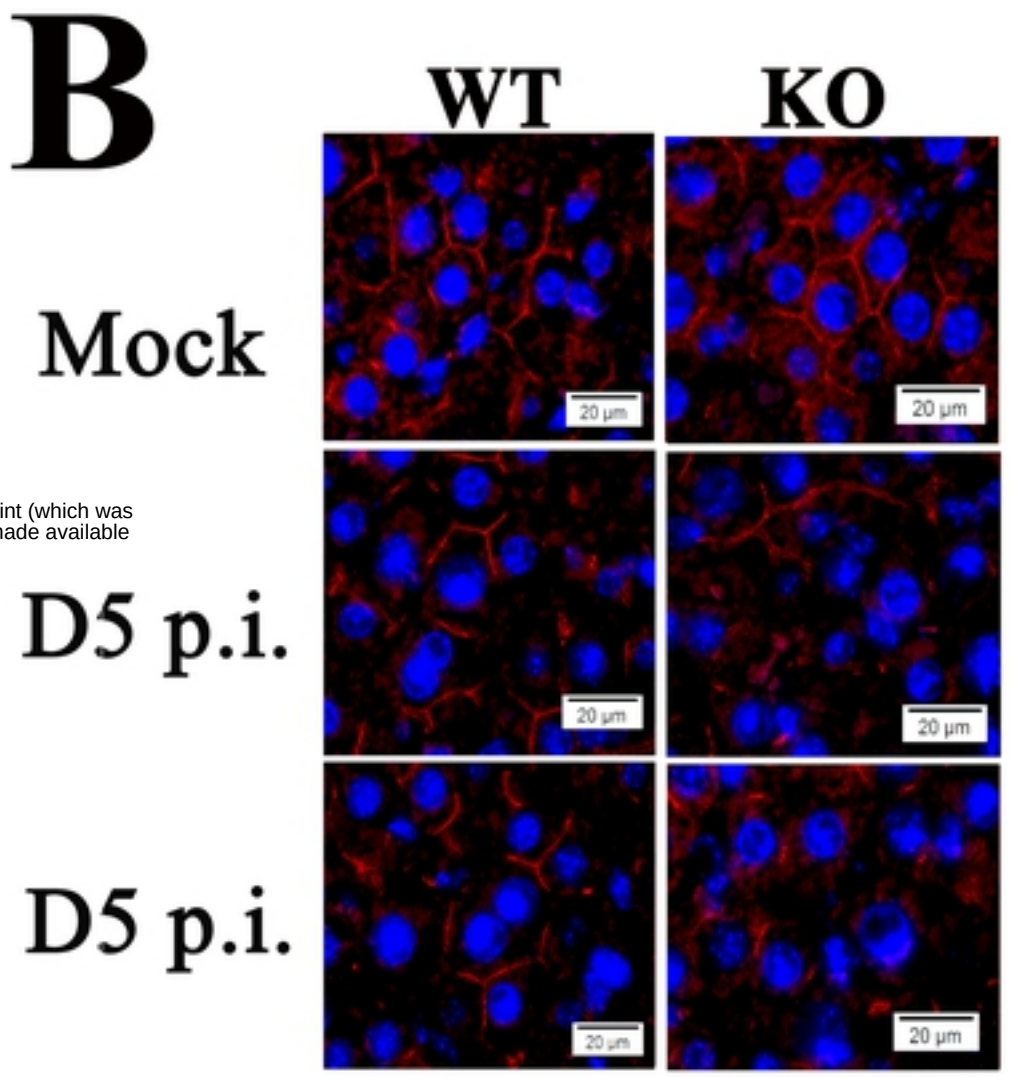

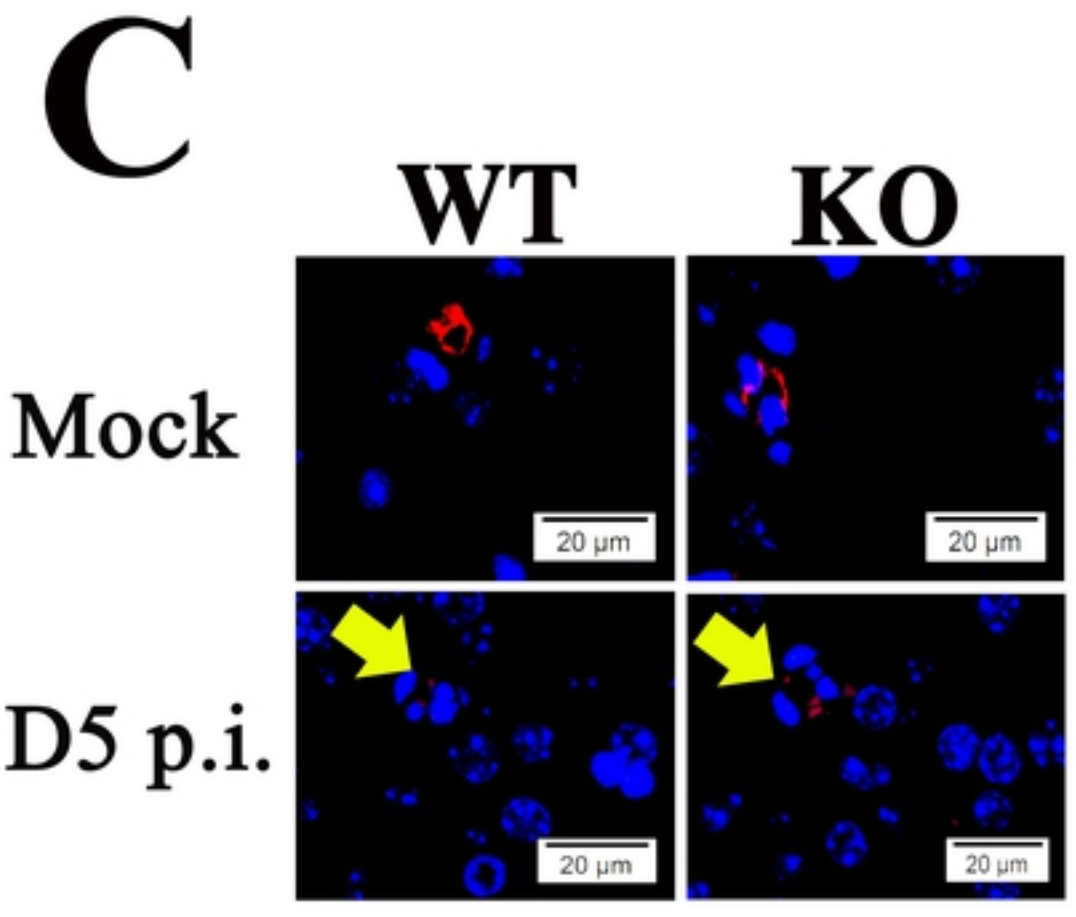

Fig 8

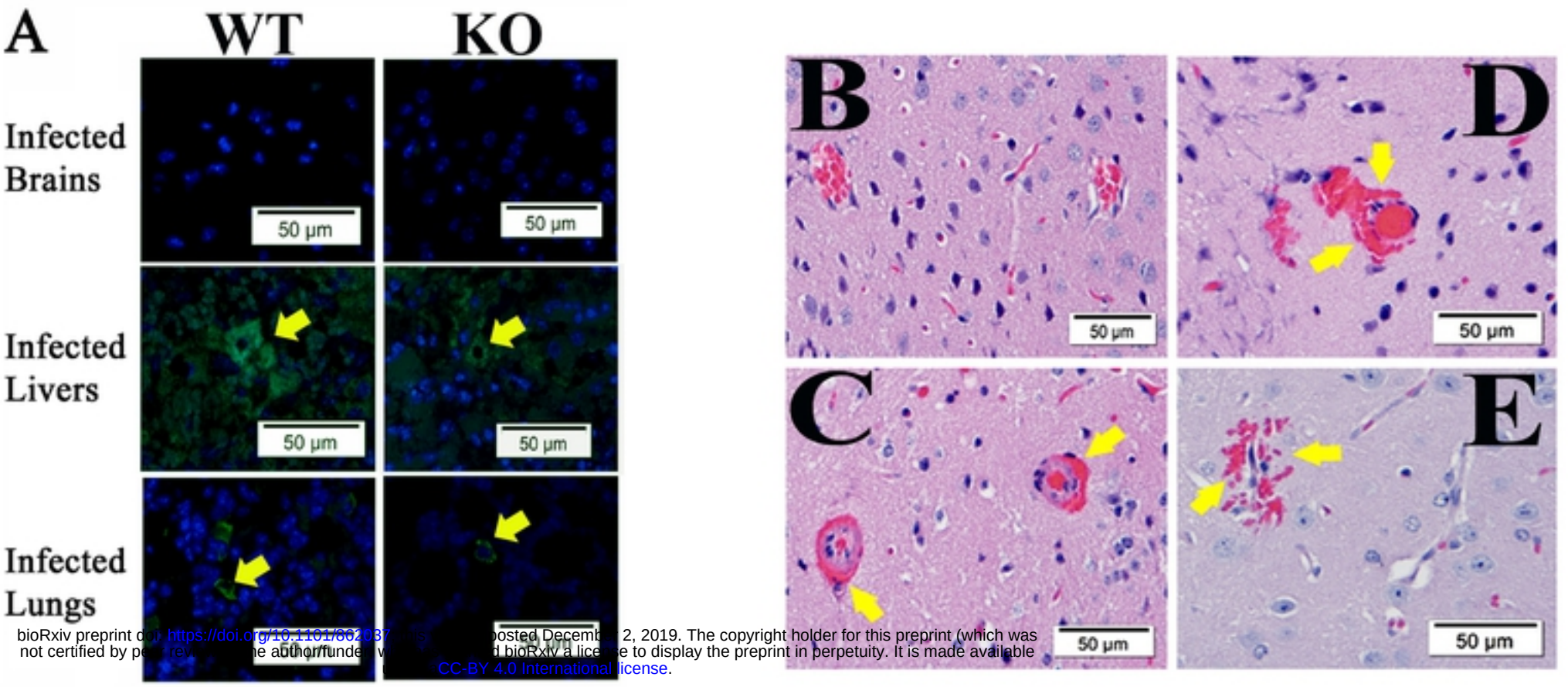

Fig 9